Review

Raman Spectroscopy and Its Application in Fruit Quality Detection

Yong Huang [1], Haoran Wang [1] , Huasheng Huang [1], Zhiping Tan [1], Chaojun Hou [2], Jiajun Zhuang [2] and Yu Tang [1,*]

1   Academy of Interdisciplinary Studies, Guangdong Polytechnic Normal University, Guangzhou 510665, China; gsdhuangy@gpnu.edu.cn (Y.H.); 15537470396@163.com (H.W.); huanghsheng@gpnu.edu.cn (H.H.); tanzp@gpnu.edu.cn (Z.T.)
2   College of Mathematics and Data Science, Zhongkai University of Agriculture and Engineering, Guangzhou 510225, China; houchaojun@zhku.edu.cn (C.H.); zhuangjiajun@zhku.edu.cn (J.Z.)
*   Correspondence: yutang@gpnu.edu.cn

Abstract: Raman spectroscopy is a spectral analysis technique based on molecular vibration. It has gained widespread acceptance as a practical tool for the non-invasive and rapid characterization or identification of multiple analytes and compounds in recent years. In fruit quality detection, Raman spectroscopy is employed to detect organic compounds, such as pigments, phenols, and sugars, as well as to analyze the molecular structures of specific chemical bonds or functional groups, providing valuable insights into fruit disease detection, pesticide residue analysis, and origin identification. Consequently, Raman spectroscopy techniques have demonstrated significant potential in agri-food analysis across various domains. Notably, the frontier of Raman spectroscopy is experiencing a surge in machine learning applications to enhance the resolution and quality of the resulting spectra. This paper reviews the fundamental principles and recent advancements in Raman spectroscopy and explores data processing techniques that use machine learning in Raman spectroscopy, with a focus on its applications in detecting fruit diseases, analyzing pesticide residues, and identifying origins. Finally, it highlights the challenges and future prospects of Raman spectroscopy, offering an effective reference for fruit quality detection.

Keywords: Raman spectroscopy; machine learning; detection of fruit diseases; detection of fruit pesticide residues; identification of fruit origin

1. Introduction

With the advancement of modern agriculture, fruits have become essential sources of essential nutrients due to their rich content of minerals, vitamins, and dietary fibers [1]. However, fruit diseases caused by pathogenic bacteria and the use of excessive pesticides have led to pesticide residues in fruits, posing a significant threat to human life and health, affecting fruit sales in different regions, and presenting a major challenge to the sustainable development of the fruit industry [2–4]. To detect and identify the quality of fruits, various methods have been applied, including sensory evaluation, Polymerase Chain Reaction (PCR) detection, Gas Chromatography-Mass Spectrometry (GC-MS) detection, spectral detection, and others. Sensory evaluation is suitable for evaluating both the external and certain internal qualities of fruits, such as freshness, ripeness, and internal defects, which are of particular concern [5]. PCR detection, which is known for its high stability and accuracy, is effective in identifying the DNA or RNA of pathogens and detecting gene mutations associated with genetic diseases. Recently, real-time quantitative PCR (qPCR), multiplex PCR (mPCR), and digital PCR (dPCR) have amplified specific DNA segments in a shorter time, offering the potential for precise diagnosis and immediate detection [6].

GC-MS, known for its high separation efficiency and rapid analysis, is primarily used to detect organic pollutants in water or soil and analyze bioactive compounds in plants. Recently, the adoption of triple quadrupole GC-MS and the HES 2.0 ion source has allowed for the detection of compounds at extremely low concentration levels, which is crucial for applications requiring exceptionally high sensitivity [7].

Spectral analysis has been extensively utilized in fruit quality detection, biomedical identification, and environmental monitoring due to its high sensitivity, resolution, and non-destructive nature. According to the detection wavelength and excitation source, the types of spectroscopy applied include infrared (IR), near-infrared (NIR), and Raman spectroscopy (RS), among others. IR and NIR spectroscopy facilitate both qualitative and quantitative analysis of samples. The advancement of techniques, such as two-dimensional material-polariton-enhanced infrared spectroscopy, MoO_3 phonon-polariton-enhanced infrared spectroscopy, and surface-enhanced infrared spectroscopy, has significantly amplified molecular vibrational absorption signals, thereby improving detection sensitivity [8,9]. Compared with IR and NIR spectroscopy, Raman spectroscopy demonstrates strong applicability, including resistance to moisture interference and minimal consumption of chemical reagents, particularly when combined with laser techniques that offer high monochromaticity and strong directivity. High-sensitivity detectors and confocal microscopes have improved their capabilities, so RS has become a widely adopted analytical tool in the field of fruit quality detection [10]. This review focuses on the application of Raman spectroscopy combined with machine learning for the rapid and non-destructive analysis of fruit quality. It introduces the principles and recent advancements in Raman spectroscopy detection techniques that use machine learning algorithms and then provides a comprehensive overview of Raman spectroscopy applications in fruit disease, pesticide residue detection, and origin identification. Finally, the challenges and future trends of Raman spectroscopy for non-destructive and rapid fruit quality analysis are discussed. This review aims to provide new perspectives and pave the way for the future application of Raman spectroscopy in fruit quality detection.

2. Main Techniques of Raman Spectroscopy

2.1. Principle of Raman Spectroscopy Technique

In spectroscopy detection, the photons emitted by the laser interact with the electron clouds and molecular bonds in the sample, leading to Rayleigh scattering and Raman scattering. The excited molecules transition from the ground state to a higher-energy excited state and then return to other vibrational levels. This process is divided into Stokes Raman scattering, in which the photon energy decreases from $h\nu_0$ to $h\nu_0 - h\nu_m$, and anti-Stokes Raman scattering, in which the photon energy increases from $h\nu_0$ to $h\nu_0 + h\nu_m$. The electron energy level transitions for Raman and Rayleigh scattering are shown in Figure 1 [11–13]. According to the Boltzmann distribution, molecules in the ground state are more stable in thermal equilibrium; thus, most molecules are in this state. Because Stokes Raman scattering involves transitions from the ground state, its probability is higher than that of anti-Stokes Raman scattering.

The intensity of the Raman signal depends on the concentration, enabling quantitative analysis [14]. The relation between these parameters can be expressed as

$$I_R \propto v^4 I_0 N \left(\frac{\partial \alpha}{\partial \phi} \right)^2 \tag{1}$$

where ν is the frequency of the incident laser radiation, I_0 is the intensity of the incident laser radiation, N is the number of scattering molecules in a given state, α is the polarizability of the molecules, and ϕ is the amplitude of the molecular vibration.

During Raman scattering, changes in photon energy produce Raman shifts that arise

from alterations in molecular vibrations or spin states. Correspondingly, the stretching vibrations and spin states of molecular chemical bonds can be analyzed using Raman spectroscopy. Initially, Raman spectroscopy was applied to detect hydrogen bonds but has since been advanced to identify covalent bonds, such as $C-C$, $-C=C-$, $N-O$, and $C-H$ bonds [15]. For instance, carotenoids in citrus fruits exhibit three prominent Raman characteristic peaks at Raman shifts of 1003 cm^{-1}, 1155 cm^{-1}, and 1520 cm^{-1}, corresponding to $-C=C-$bond stretching vibration, $C-C$ bond stretching vibration, and in-plane CH_3 vibrations, respectively, as shown in Figure 2 [16]. Changes in the content of organic compounds can be assessed by analyzing the position and intensity vibrations at these peaks. During the acquisition of Raman spectra, interference from ambient light and temperature variations significantly affects the results. Ambient light introduces additional signals to the detector, which are superimposed on the true Raman spectrum, leading to increased background noise and a reduced signal-to-noise ratio. Therefore, background light sources should be shielded during measurements and eliminate the interference of background light in the spectrum. The optical components of spectrometers should be operated at their designed working temperature. Temperature variations affect the refractive index of optical elements, the optical path, and focusing performance. Thus, it is essential to acquire spectra under constant temperature conditions [17,18]. The Raman signal generation process involves photons emitted by the laser being refracted onto the sample through a dichroic mirror. The scattered light is then filtered and transmitted to the spectrometer through a dichroic mirror and a filter. Finally, the beam is focused on the detector, where the collected signal is converted into an electrical signal [19]. The configuration of the Raman spectrometer is illustrated in Figure 3.
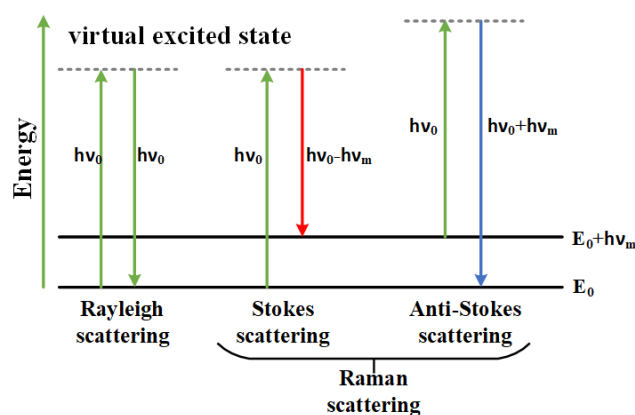

Figure 1. Electron energy level diagram illustrating Rayleigh scattering and Raman scattering processes.
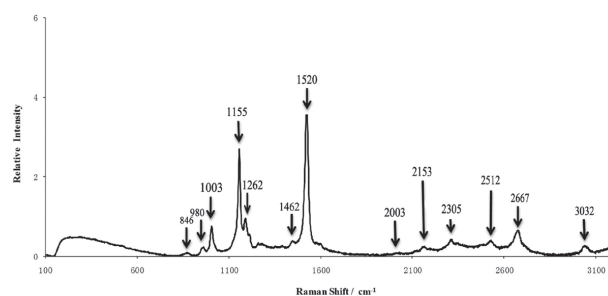

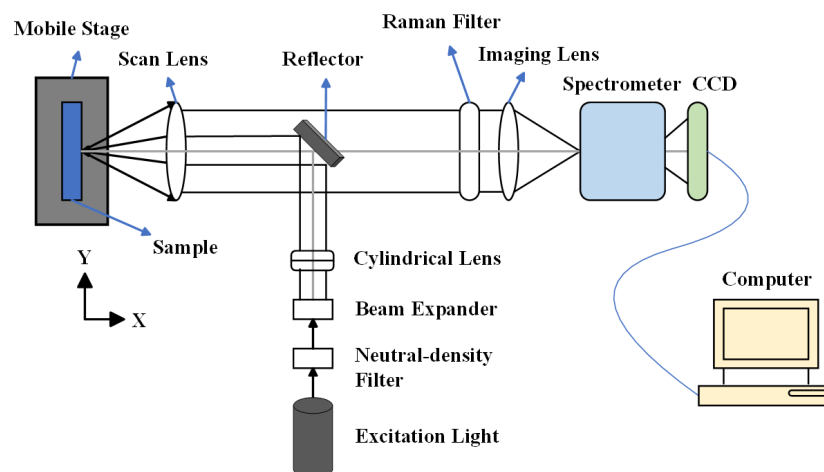**Figure 2.** Raman spectrum of citrus peels.

Figure 3. Structure diagram of Raman spectrometer.

The intensity of the Raman spectral signal is very low in the absence of an enhancement mechanism; thus, it is especially difficult to obtain Raman spectral information from the interior of the sample, as Raman spectra are typically generated when the surface interacts with incident light. In addition, the scattering cross-section of most molecules is very small, and they can produce a strong fluorescence background under laser irradiation, which interferes with the Raman signal and makes it more difficult to capture [20]. To overcome these challenges in Raman spectroscopy, advanced spectral techniques, such as Surface-Enhanced Raman Spectroscopy (SERS), Confocal Micro-Raman Spectroscopy (CM-RS), and Spatially Offset Raman Spectroscopy (SORS), have been increasingly adopted [21].

2.2. Surface-Enhanced Raman Spectroscopy

To enhance the intensity of the Raman signal, target molecules are adsorbed onto the substrate surface of metal nanoparticles (NPs) due to the surface plasmon resonance effect of metal NPs and the charge transfer between molecules and metals, as shown in Figure 4, in which both physical and chemical enhancement mechanisms amplify the Raman scattering intensity by up to 10^{14}-fold. However, the intensity is amplified only 10^4- to 10^6-fold in the absence of NPs [22,23]. Table 1 presents the optimal types and morphologies of metal substrates for detecting fruit compounds utilizing the SERS technique. Metal substrates play a crucial role in SERS, so the preparation of metal substrates is essential for achieving Raman signal enhancement. Usually, substrates can be prepared using methods such as electrochemical deposition, vacuum evaporation, and metal colloids [24–26]. When prepared using electrochemical deposition, such substrates are suitable for the detection of pollutants and non-adsorbent analytes in air, soil, and water, but they often exhibit uneven distribution and limited flexibility. The metal film deposited by vacuum evaporation for SERS substrates is suitable for materials such as Polymethylmethacrylate (PMMA), Polyvinylidene Fluoride (PVDF), Polydimethylsiloxane (PDMS), Polyethylene Terephthalate (PET), and proteins. Alternatively, the periodic folded gold nanostructure SERS substrates and flexible SERS substrates prepared using metal colloids are suitable for detecting additives, pesticide residues, mycotoxins, and other contaminants in food.

The preparation of periodic folded nanosubstrates utilizes AFM dynamic lithography and nano-cutting techniques to precisely control the periods and nanogap widths of the folded nanostructures, thereby optimizing the surface plasmon resonance effect to enhance the Raman signal. The SERS technique based on periodic folded gold nanoparticles has been applied in the detection of organic compounds in the substrate. Ye et al. [27] designed periodic folded gold nanostructure substrates that exhibit the three-dimensional nano-focusing effect, hotspot effect, and standing wave effect, creating an extremely high

electromagnetic field to enhance the Raman signal. The minimum detection limit for paminothiophenol (PATP) in the substrate reached 10^{-9} M. When this substrate was not applied, Zhang et al. [28] employed the SERS technique using IP6@Au with Fe^{3+} as a reinforcing agent. The minimum detection limit of 10^{-7} M for PATP on the substrate was achieved.

The preparation of flexible substrates deposits plasma nanomaterials onto the surface of supporting materials, such as polyvinyl alcohol, cellulose, and biofilm. When the substrate is bent and folded, the flexibility and thermal stability remain excellent, allowing it to be applied in various shapes. SERS based on flexible materials has been widely applied in the detection of food-borne pathogens and vitamins in food. Due to the abundance of hydroxyl groups on cellulose, silver nanoparticles easily bind to celluloses, forming a bendable SERS chip. Pham et al. utilized this SERS chip to detect thiram residues in apples, achieving a minimum detection limit of 1.01×10^{-8} M. As the concentration decreases from 1.0×10^{-3} M to 1.0×10^{-9} M, the peak intensity gradually diminishes on rigid substrates, whereas the peak intensity of flexible substrates remains clearly observable within this range. The corresponding Raman spectra are shown in Figure 5 [29]. SERS can achieve single-molecule detection, with detection limits as low as 1.0×10^{-9} M or even lower in certain cases, making it highly suitable for applications in biomedical and food safety detection.
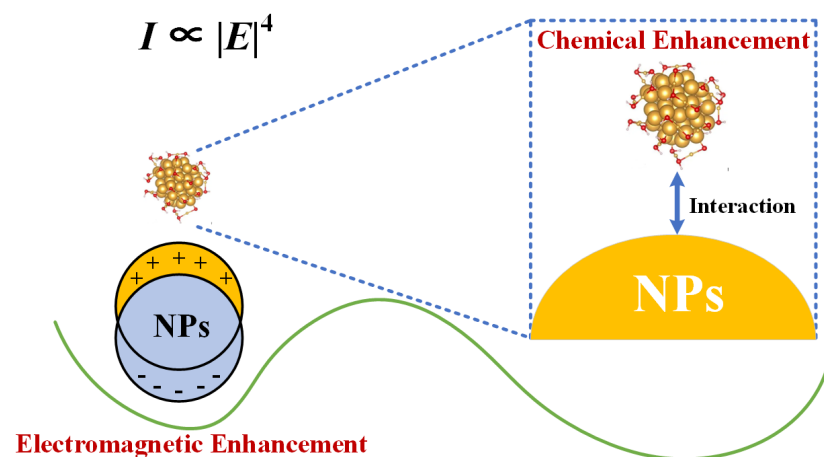

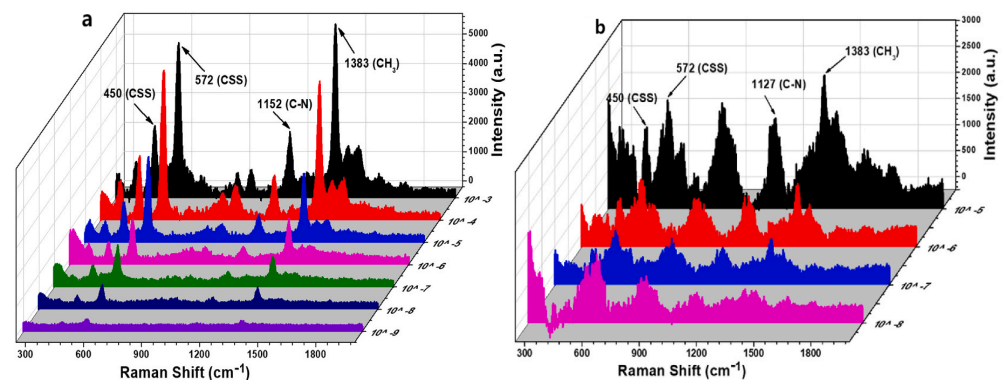**Figure 4.** Enhancement mechanism of SERS.

Figure 5. (**a**) SERS spectra of thiram solution at different concentrations on rigid Ag/Al substrate, (**b**) SERS spectra of thiram solution at different concentrations on flexible PVA/cellulose/Ag chips.

Table 1. Optimal types and morphologies of metal substrates for SERS detection of various fruit compounds.

Sample	Internal Compounds	Metal Substrate Type	Substrate Morphology
Citrus	Hesperidin, Tangeretin	Au	Nanoparticles
	Coumarin, D-Limonene, β-Carotene	Ag	Nanotrees
Apple	Quercetin, Malic Acid, Citric Acid	Au	Nanoparticles
	Fructose, Glucose, Sucrose, Vitamin C	Ag	Nanoparticles
Tomato	Benzo-a-pyrene	Au	Nanofilms
	Coumarin, D-Limonene, β-Carotene	Ag	Nanofilms
Grapefruit	Ethy1 Acetate, Naringin	Au	Nanoparticles
	Limonene, Sucrose, β-Carotene	Ag	Nanotrees
Cherry	phenethyl alcohol, Ethyl Acetate	Au	Nanoparticles
	Anthocyanin, Citric Acid, Glucose, Fructose	Ag	Nanoparticles
Pear	Hexanal, Ethyl Acetate	Au	Nanoparticles
	Fructose, Glucose, Malic Acid	Ag	Nanoparticles
Lemon	Hesperetin, Limonene	Au	Nanoparticles
	Citric Acid, Vitamin C	Ag	Nanoparticles
Strawberry	Anthocyanin, Quercetin, Hexyl Acetate	Au	Nanoparticles
	Fructose, Glucose, Citric Acid, Vitamin C	Ag	Nanoparticles
Grape	Quercetin, Hexyl Acetate	Au	Nanospheres
	Fructose, Glucose, Tartaric Acid	Ag	Nanospheres

2.3. Confocal Micro-Raman Spectroscopy

Confocal Micro-Raman Spectroscopy (CM-RS) combines the high-resolution imaging capability of confocal microscopy with the chemical analysis capability of Raman spectroscopy by aligning the laser light source, sample, and detector to effectively filter out stray light from the defocused regions of the sample. Initially, CM-RS had a spatial resolution in the range of 0.5 to 1 μm. With the introduction of methods such as near-field Raman spectroscopy (NRS) and time-resolved Raman spectroscopy (TRS), the spatial resolution of micro-Raman spectrometers has been significantly enhanced, reaching levels as low as several nanometers and even achieving tens of nanometers [30], with the structure of the spectrometer illustrated in Figure 6 [31]. Due to the limited polarization capability of the CM-RS spectrometer, a spectrometer with polarization capability provides symmetry information of molecular vibrations within the Raman spectra, aiding in the identification and characterization of molecular structures.

Acher et al. enhanced the microscope with a polarization analysis capability, as shown in Figure 7. In Raman polarization experiments conducted on silicon, they observed an IX-Pol/ICo-Pol ratio of 0.61 with a standard deviation of 2%. This device enables simultaneous measurement of both co-polarization and cross-polarization Raman spectra, allowing

for the acquisition of "unpolarized" Raman spectra alongside polarization information. This capability is particularly valuable for studying the crystal orientation and stress state of anisotropic samples [32].

Figure 6. Structure diagram of a confocal micro-Raman spectrometer.

Figure 7. Structure diagram of Raman microscope with polarization analysis capability.

2.4. Spatially Offset Raman Spectroscopy

To detect Raman signals in the interior of a sample, Spatially Offset Raman Spectroscopy (SORS) acquires molecular structure information at depth by adjusting the spatial offset between the laser source focal point and the lens focal point, as shown in Figure 8. The first recorded depth for SORS was 3 mm. Recent advancements in the technique have demonstrated that the detection depth can now reach up to 5 cm. SORS can detect information in the interior of a sample without contacting it but cannot enhance the Raman signal [33–35]. In contrast, Inverse Spatially Offset Raman Spectroscopy (ISORS) applies a conical lens to generate a ring-shaped beam, with the ring radius precisely controlled by varying the distance between the lens and the sample, achieving Raman signal enhancement.

McMillan et al. applied the ISORS technique to offset the collection point of the Raman spectra away from the laser incident point, effectively reducing fluorescence background interference, as shown in Figure 9 [36]. Utilizing this technique, the Raman signal intensity and signal-to-noise ratio for samples obstructed by glass bottles were increased threefold compared to the original method. The SORS technique enables the detection of Raman

information from deeper layers within samples, making it suitable for applications in biomedical research and agricultural product analysis.
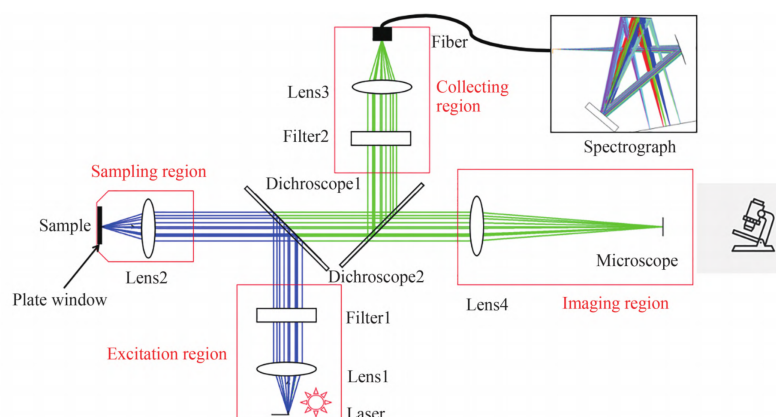

Figure 8. Structure diagram of a spatially offset Raman spectrometer.
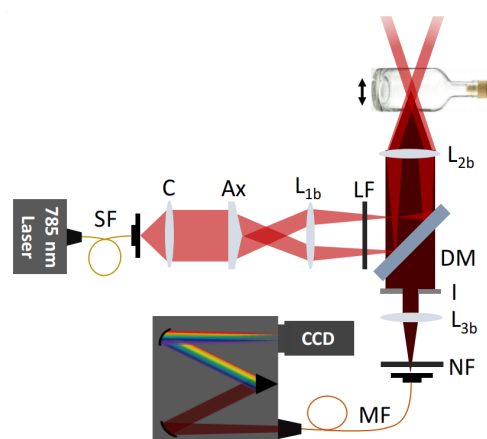

Figure 9. Raman spectrum device diagram of a sample in a glass bottle collected by ISORS.

In addition, Fourier-Transform Raman Spectroscopy, Tip-Enhanced Raman Spectroscopy, and Stimulated Raman Spectroscopy improve the signal-to-noise ratio, enhance Raman signal intensity, and achieve high spatial resolution. In recent years, various models of Raman spectrometers have been developed, and suitable Raman spectrometers can be selected according to the chemical composition of the sample, spectral resolution, and experimental conditions. Consequently, various Raman spectrometers, as non-destructive, highly sensitive, and versatile analytical tools, have been extensively applied across fields such as food safety, materials science, and life sciences. Table 2 presents several Raman-related technical principles and applications. Table 3 presents the excitation wavelengths, spectral ranges, and resolutions of different Raman spectrometers.

Different excitation source wavelengths are applied in Raman spectrometers, which range from ultraviolet (UV) to near-infrared (NIR) and even further. According to the sample absorption characteristics and spectral resolution, different excitation wavelengths should be applied. The light scattering intensity, background fluorescence, and acquisition time are affected by the excitation wavelength. For example, ultraviolet excitation wavelengths range from 100 to 400 nm. They have strong Raman scattering and are suitable for organic biological samples, such as proteins, nucleic acids, and biofilms, due to their resonance with ultraviolet excited light to enhance the Raman signal [37].

Table 2. Summary and comparison of Raman-related techniques.

Raman Related Technique	Principle	Advantages and Disadvantages	Application	References
Traditional Raman Spectroscopy	The frequency of the scattered photon is different from that of the incident photon.	Non-moisture interference; non-destructive. Raman signal is weak and susceptible to fluorescence interference.	Materials science, life sciences, criminal investigation, forensic science	[11–13]
Surface-Enhanced Raman Spectroscopy	Uses interactions between molecules and coarse metal nanoparticles to enhance Raman signals.	High sensitivity; enhanced Raman signal. Substrate-dependent; susceptible to fluorescence interference	Food safety testing, nanoscale manufacturing technology	[22,23]
Confocal Micro-Raman Spectroscopy	Combines the spatial resolution of the microscope with the molecular vibrational power of Raman spectroscopy.	High spatial resolution; no interference from fluorescent background. High sample preparation requirements.	Biomedical, geological, mineralogical	[30,31]
Spatially Offset Raman Spectroscopy	The scattered light at different depths of the sample produces different shifts.	Deep signal detection; remote control. Technical complexity.	Medical diagnosis, environmental monitoring	[33–35]
Fourier-Transform Raman Spectroscopy	Converts the signal in the time domain to the frequency domain.	High signal-to-noise ratio; wide measurement band. Sample photosensitivity.	Chemical analysis, pharmaceutical research	[38,39]
Tip-Enhanced Raman Spectroscopy	An intensity electromagnetic field generated near the tip of a metal nanostructure is utilized.	High sensitivity; strong applicability. High precision of needle tip preparation.	Electrochemical interface, biological interface	[40,41]
Stimulated Raman Spectroscopy	Nonlinear interactions between molecules and lasers.	High chemical specificity. Expensive equipment.	Materials science, medical diagnostics	[42,43]

Table 3. Summary and comparison of different models of Raman spectrometers.

Model	Company and Location	Excitation Wavelength (nm)	Spectral Range (cm^{-1})	Resolution (cm^{-1})
Progeny	Rigaku; Japan	1064	200–2500	8–11
BRAVO	Bruker; Germany	785, 852	300–3200	10–12
Resolve	Agilent; America	830	300–3200	5–10
Virsa[tm]	Renishaw; Britain	532, 785	50–4000	<250

Table 3. *Cont.*

Model	Company and Location	Excitation Wavelength (nm)	Spectral Range (cm^{-1})	Resolution (cm^{-1})
ReactRaman 802L	Mettler Toledo; Switzerland	785	150–3400	4–6
i-Raman Prime 785H	Metrohm AG; Switzerland	785	150–2800	<6
NRS-5000/7000	Jasco; Japan	532, 785, 1064	5–8000	0.3–0.4
MINI CCT+	Horiba Scientific; France	532, 660, 785	210–3500	8–12
B&W TEK I-RAMAN	Spectra Research Corporation; America	532, 785	65–4000	3.5–4.5
Cora 5001	Anton Paar GmbH; Austria	532, 785, 1064	100–3500	6–9

3. Data Processing and Analysis

The molecular structural information obtained from Raman spectral data facilitates structural characterization and substance identification, which are beneficial for both quantitative and qualitative analysis. Data preprocessing improves the quality of the spectra, while post-processing emphasizes feature extraction and modeling with the preprocessed data, reducing computational complexity and enhancing analytical efficiency [44].

3.1. Spectral Pretreatment

The fluorescent backgrounds and cosmic spikes caused by optical effects and the detector response characteristics of the Raman spectrometer lead to multiple overlaps or similar spectral features. Therefore, raw Raman spectra require preprocessing, such as spike correction, baseline correction, and smoothing, to ensure accurate identification of the analyte [45,46].

3.1.1. Spike Correction

The detector in a Raman spectrometer is a charge-coupled device (CCD) that can detect high-energy charged particles from outer space while capturing scattered light. This results in Raman spectra with random, unidirectional, narrow, and sharp peaks, which are misinterpreted as true Raman peaks. Therefore, a spike correction for the Raman spectra is necessary [47]. Spike correction is divided into three categories. The first category involves repetitive collection, such as robust summation and upper-bound spectra, which require at least two spectra to be collected and are unsuitable for dynamic detection [48]. The second category focuses on hardware improvements to enhance the performance of optical detection devices, and, compared to theoretical methods, these approaches are more complex and costly [49]. The final category is single-spectral detection, including techniques such as median filtering and interpolation filtering.

Median filtering and interpolation filtering replace the peaks of the Raman signals with the median or interpolated values of the points, within a specified interval centered on the target point, to eliminate noise. Median filtering effectively removes impulse noise, as its working principle aligns with the characteristics of impulse noise; however, it falls short in preserving image edge details. In contrast, interpolation filtering preserves image details by increasing pixel points without altering the features of the image, addressing random pulse interference and other types of noise with greater flexibility [50]. Mosafapour et al. [46] performed

preprocessing on the Raman spectra of six substances, including ethanol and acetonitrile. The average values and standard deviations of the spectra processed with interpolation filtering were lower than those of the raw spectra, and the classification accuracy of the six substances reached 100% by establishing a PCA-LDA model.

3.1.2. Baseline Correction

When laser light irradiates a sample, fluorescent materials within the sample absorb photons and emit fluorescence, causing baseline drift in the Raman spectrum. Fluorescent interference obscures the correct spectral distribution, affecting the identification and analysis of Raman peaks. Baseline correction is employed to restore the raw spectrum, with common approaches including polynomial fitting and multivariate scatter correction [51,52].

Polynomial fitting and multivariate scatter correction remove the baseline through mathematical calculations [53,54]. However, when the fluorescence signal is excessively strong, the fluorescence background may overlap with the Raman signal, making it challenging to separate the two, and mathematical approaches alone may not be sufficient to remove the baseline. In such cases, optimization of the detection instrument must be performed before spectral collection. Optimization techniques include time-gated Raman spectroscopy [55], modulated Raman spectroscopy [56], and shifted excitation Raman difference spectroscopy (SERDS) [57]. All three optimization techniques improve the signal-to-noise ratio, but there are differences: time-gated Raman spectroscopy reduces fluorescence interference by utilizing time differences, modulated Raman spectroscopy enhances the Raman signal by modulating the light source, and SERDS adjusts the wavelength shift to eliminate the fluorescence background.

3.1.3. Smoothing

Fixed noise, emission noise, and background noise in the spectrometer cause random fluctuations in the Raman signal, affecting peak shapes and data accuracy [58]. Spectral smoothing can reduce signal fluctuations and ensure the continuity of the signal. Common smoothing approaches include moving-window averaging, the wavelet transform (WT), and the Savitzky–Golay (SG) algorithm.

Moving-window averaging requires setting a window that moves from the far left to the far right of the spectral curve. However, this method is subjective in determining the window size, and edge effects occur during the window movement, leading to inconsistent smoothing results [59]. The wavelet transform (WT) is a time-frequency analysis technique in which wavelet functions decompose the signal into wavelet coefficients, allowing the capture and reconstruction of signal features [49]. The WT is particularly effective at handling complex noise. For instance, Pan et al. [60] applied a WT-DCNN classifier to mixed noise data containing Gaussian noise and baseline noise, achieving the highest classification accuracy, outperforming the KNN and SVM models. The SG algorithm requires setting the polynomial order and window size. It performs least-squares fitting based on a polynomial function within the filtering window, smoothing the spectral data point by point [61]. Yuan et al. [62] developed a KNN classification model for plastics, where accuracy improved from 79.83% to 88.15% after applying SG smoothing to the data.

3.2. Data Post-Processing

Data post-processing extracts the characteristics and information affecting the change in the spectral intensity from the preprocessed data and establishes a qualitative or quantitative analysis model. Machine learning can learn patterns and associations from data, adapting to complex and ever-changing data environments, so it performs data post-processing processes efficiently.

3.2.1. Feature Extraction

The preprocessed spectral data typically exhibit high dimensionality and contain irrelevant information. Raman spectral feature extraction algorithms can identify changes in Raman intensity within characteristic bands, significantly reducing data redundancy and improving the signal-to-noise ratio [63]. Commonly used Raman spectral feature extraction methods include Principal Component Analysis (PCA), Successive Projections Algorithm (SPA), and Competitive Adaptive Reweighted Sampling (CARS) [64]. Table 4 presents a summary and comparison of these three Raman feature extraction algorithms, which are described as follows:

- Principal Component Analysis Algorithm

PCA is an unsupervised feature extraction algorithm that projects high-dimensional data matrices onto a lower-dimensional space, selecting independent variables with the greatest variance contribution as the principal components. This algorithm reduces dimensionality while retaining information from the original data [65]. In the detection of apple valsa canker, Zhao et al. [66] utilized the PCA algorithm to perform a linear combination of independent variables from the raw Raman spectral data and ranked them based on their variance contribution rates. The first two principal components achieved a cumulative contribution rate of 99.38%. By analyzing the correlation between the principal components and the original variables (x-loadings), the Raman spectral feature wavenumbers were reduced from 994 to 5, thereby extracting wavenumbers closely related to the disease. This reduction in data dimensionality not only avoided model overfitting but also improved the model's generalization ability and accuracy. However, when the data contain noise or the dataset is large, PCA's ability to calculate variance is affected, leading to increased computational costs.

The Robust PCA (RPCA) algorithm recovers low-rank data from the original data and is used to process noisy data. Pulpito et al. applied this algorithm to the online detection of moving targets in noisy ocean scenes. When the recall rate was 80%, the accuracy of the S-OMW-RPCA algorithm surpassed that of the original OMW-RPCA algorithm [67]. For large datasets, the 2DPCA algorithm operates in the two-dimensional space of the data without converting the data matrix into a one-dimensional vector. Jiang et al. [68] utilized the 2DPCA algorithm to reduce the dimensionality of large-scale face recognition images. The results indicated that the image quality processed with the 2DPCA algorithm was significantly higher than that processed with the standard PCA algorithm.

- Successive Projections Algorithm

SPA is a feature extraction algorithm based on forward iterative search, where in each iteration, the wavelength with the maximum projection value is selected as the new variable until the number of selected variables reaches the predefined value [69]. The SPA algorithm performs well in handling large datasets and reducing redundant information. However, as it performs only a single-layer projection, it is insufficient for optimizing the model's prediction performance.

The DLV-SPA algorithm analyzes independent and dependent variables at the latent variable projection layer, minimizing the independence or linear correlation between two adjacent wavelengths, thereby improving model performance. Chen et al. [70] applied the DLV-SPA algorithm to a quantitative detection model of fish meal ash, and the results showed that the standard deviation of the model was 1.78, compared to 2.82 for the traditional chemical method.

- Competitive Adaptive Reweighting Sampling Algorithm

CARS is a feature variable extraction algorithm that combines Monte Carlo sampling with Partial Least Squares (PLS) regression coefficients. It employs an exponential decay

function and adaptive reweighted sampling to select the optimal subset of characteristic wavelengths, minimizing cross-validation error. The CARS algorithm can eliminate non-informative and collinear overlapping variables, improving the predictive capability and interpretability of the model [71]. However, data processed with this algorithm are affected by non-resonant background interference.

The Learning Discrete Hilbert Transform (LeDHT) generates analytic signals from real-valued signals. Adjusting the signal phase in the frequency domain resolves the discrepancies between the measured and actual values caused by distortion. Camp et al. [72] applied the LeDHT to the Raman retrieval problem for representative Dawson function spectra, and the results showed that the Mean Squared Error (MSE) of the LeDHT algorithm was 10^{-8} au, which was lower than that of the traditional DHT Pad and DHT algorithms.

Table 4. A summary and comparison of the three Raman feature extraction algorithms.

Algorithm	Principle	Advantages and Disadvantages	Computational Complexity	Stability	Interpretability
PCA	Utilizes linear transformation to convert original variables into uncorrelated variables (principal components), ranked by variance contribution.	Does not require label information; simple computation. Sensitive to noise; requires manual determination of the number of components.	Low	High	Low
SPA	Selects variables step by step by projection to maximize independence between variables.	Highly adaptable. Computationally intensive; dependent on model selection.	Medium	High	Low
CARS	Combines Monte Carlo sampling and PLS regression coefficients to adaptively reweight and select variables.	Handles nonlinear relationships; suitable for large datasets. Computationally complex; complex parameter selection.	High	High	Low

3.2.2. Model Establishment

Due to the interactions between sample components, the acquired spectra are not superpositions of the individual component spectra, making the spectral data difficult to classify and regress. Machine learning unveils patterns and relationships within the data, encompassing three learning paradigms: supervised, unsupervised, and semi-supervised learning. The machine learning algorithms utilized to establish the model include Linear Discriminant Analysis (LDA), partial least squares discriminant analysis (PLS-DA), and

Support Vector Machine (SVM), among others [73]. Table 5 presents a summary and comparison of these three model-establishing algorithms, which are described as follows:

- Linear Discriminant Analysis Algorithm

    LDA is a supervised classification algorithm that divides the feature space into two regions and projects the training set onto a linear discriminant function, maximizing inter-group differences while minimizing intra-group differences, thereby achieving dimensionality reduction and data classification [74]. However, as the complexity of integrated circuits increases, the LDA algorithm does not optimize testing time or costs.

    By reducing the eigenvalues, ranking the eigenvectors, and selecting those associated with significant eigenvalues as inputs, both the testing time and costs are reduced. When detecting large-scale integrated circuits, Huang et al. applied this strategy to the LDA algorithm, utilizing polynomial regression functions to select effective test patterns, resulting in a 1.75-fold reduction in testing time compared to traditional methods [75].

- Partial Least Squares Discriminant Analysis Algorithm

    PLS-DA is a supervised classification algorithm based on Partial Least Squares Regression (PLSR). It centralizes and standardizes the original data to obtain independent variables and categories, and then extracts principal components by variable mapping. The PLS-DA algorithm is widely used for the classification and prediction of high-dimensional data [76].

    In recent years, Sparse Least Squares Discriminant Analysis (SLS-DA) has been employed to select the most predictive or discriminative features from the data. By applying soft-threshold optimization for feature selection, SLS-DA improves classification accuracy and reduces runtime. Afshar et al. [77] applied the SLS-DA algorithm to analyze six genomic datasets, effectively identifying and removing irrelevant features, thereby significantly reducing runtime.

- Support Vector Machine Algorithm

    SVM is a supervised binary linear classification algorithm that maps linear data to a higher-dimensional space and identifies the optimal hyperplane for data classification in the original feature space. For nonlinear data, the hyperplane is typically determined using linear, polynomial, or radial basis kernel functions, which allow data classification [78]. However, the SVM algorithm finds the optimal solution under specific constraints, which limits its application in everyday problems.

    The Smooth Support Vector Machine (SSVM) algorithm determines model parameters by solving a quadratic programming problem, simplifying the solution process for practical applications. In an attempt to address the issue of excessive constraints in early warning systems of financial crises, Yuan et al. [79] applied PCA to reduce dimensionality and established an SSVM prediction model. The accuracy rate reached 95%, outperforming the original SVM prediction model.

Table 5. A summary and comparison of the three model-establishing algorithms.

Algorithm	Principle	Advantages and Disadvantages	Computational Complexity	Stability	Interpretability
LDA	Maximizes inter-class variance and minimizes intra-class variance to cluster data of the same class while separating different classes.	Simple computation; suitable for multi-class problems. Performs poorly on nonlinear data; sensitive to noise.	Low	High	High

Table 5. *Cont.*

Algorithm	Principle	Advantages and Disadvantages	Computational Complexity	Stability	Interpretability
PLS-DA	Establishes a linear model between independent variables and response variables, maximizing differences between classes while minimizing intra-class differences.	Simple data structure. Complex parameter selection; sensitive to noise.	Medium	High	Medium
SVM	Finds an optimal hyperplane to maximize the margin between samples of different classes.	Handles nonlinear data; strong generalization ability. Computationally intensive; requires appropriate kernel function selection.	High	High	Low

4. Application of Raman Spectroscopy in Fruit Quality Detection

There are significant differences in the types of nutritional components and pesticide residue levels between healthy and abnormal fruits. Raman spectroscopy can detect these differences based on molecular vibrations, enabling high-precision detection and identification [80]. The application of Raman spectroscopy in fruit quality detection primarily includes fruit disease detection, pesticide residue analysis, and origin identification.

4.1. Application of Raman Spectroscopy in Fruit Disease Detection

Fruits infected by conidial spores of pathogens cause severe disease issues. The conidia carried by infected fruits spread in the air, increasing the risk of fruit disease. The early detection of fruit diseases ensures fruit quality and improves yield [81]. For instance, canker and Huanglongbing (HLB) have become prevalent crop diseases in citrus, grapefruit, apples, and tomatoes. High temperatures and high humidity accelerate the transmission of disease, resulting in significant yield losses and widespread crop death [82,83]. The molecular structure and composition of infected crops undergo changes, and Raman spectroscopy can detect these changes. Therefore, Raman spectroscopy is widely applied in the early detection of crop canker and Huanglongbing.

4.1.1. Early Detection of Citrus Huanglongbing by Raman Spectroscopy

HLB is a devastating disease caused by a Gram-negative bacterium. Infected citrus crops experience a rapid decline in growth, a significant reduction in fruit yield, and, in some cases, tree death. The early detection of Huanglongbing can improve citrus yield and minimize losses caused by the disease [84]. Table 6 highlights that Raman spectroscopy has garnered significant attention for detecting citrus Huanglongbing. The characteristic band distributions for certain fruits and pesticides are shown in Tables 7 and 8.

Traditional Raman spectroscopy is used for the early detection of citrus Huanglongbing (HLB), but it is prone to interference from fluorescent substances in the citrus peel, resulting in complex noise in the Raman spectra. In contrast, Confocal Micro-Raman Spectroscopy and Fourier Raman spectroscopy can effectively eliminate fluorescence background interference, accelerating disease detection. Kong et al. [85] collected Raman spectra of healthy (HE), HLB asymptomatic (HA), and HLB symptomatic (HS) citrus samples, as shown in Figure 10, with the characteristic Raman bands corresponding to those listed in

Table 7. They preprocessed the spectra using quintic polynomial fitting and normalization and developed PCA-PLS and PCA-SVM early detection models for HLB. The diagnostic accuracy for the HE, HA, and HS prediction sets exceeded 90%, while the accuracy of traditional random detection methods ranged from only 50% to 70%. The PLS-DA algorithm effectively processed high-dimensional data and identified key variables, making it suitable for the early detection of citrus HLB. Dai et al. [86] employed cubic spline interpolation and polynomial fitting to separate spontaneous fluorescence spectra from Raman spectra in mixed spectra, establishing a PLS-DA model for citrus HLB detection and achieving accuracies of 86.08%, 98.17%, and 64.75%, respectively. Among these spectra, the Raman spectra demonstrated superior qualitative analysis. Quadratic polynomial fitting can select data points from non-peak regions, improving spectral quality. Liu et al. [87] utilized data processed with quadratic polynomial fitting and developed a PLS-DA detection model, achieving 100% accuracy. A decision diagram of the optimal number of principal components (PCs) and a scatter plot of the model are shown in Figure 11.
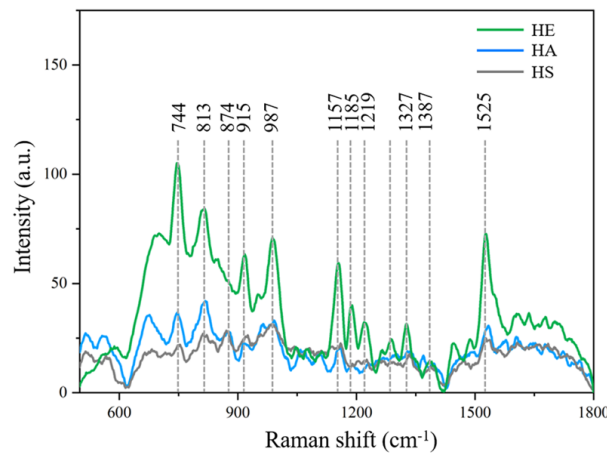
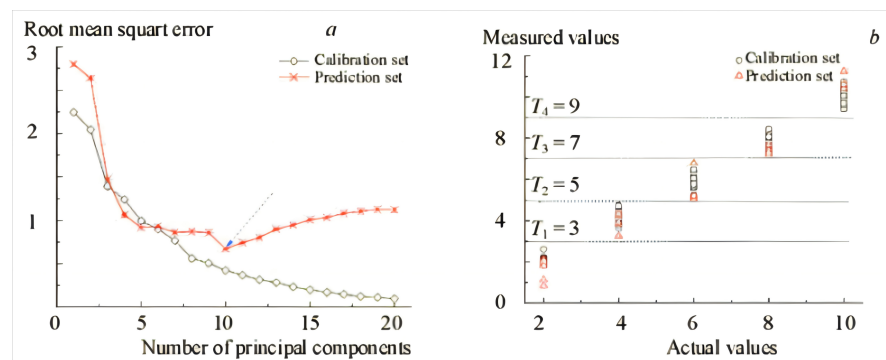**Figure 10.** Raman spectra of HE, HA, and HS citrus leaves respectively.

Figure 11. Results of the best PLS-DA model: (**a**) decision diagram of the optimal number of PCs, (**b**) scatter plot of the model.

Table 6. Application of Raman spectroscopy in the detection of citrus HLB.

Sample	Application	Algorithms	Main Result	Reference
Citrus	Huanglongbing	PCA, PLS-DA, BP-ANN	Accuracy of 97.2%, R^2 = 0.9598; RMSE = 0.0616	[88]
		PCA-PLS, PCA-SVM	Accuracies of 94.07% (PCA-PLS) and 95.56% (PCA-SVM)	[85]
		OPLS-DA	Accuracy of 89.4%	[89]
		PCA, LDA	Accuracy of 89.2%	[90]

4.1.2. Early Detection of Grapefruit Huanglongbing by Raman Spectroscopy

Grapefruit Huanglongbing is a bacterial disease transmitted primarily by insects. Insects spread the pathogen to healthy trees, causing new infections. Grapefruit trees affected by HLB exhibit yellowing of the leaves and root rot, severely threatening the grapefruit industry. Therefore, the early detection of HLB in grapefruit is essential [91].

Grapefruit has a large volume, and the storage platform of traditional Raman spectrometers cannot accommodate the entire fruit, preventing the collection of the complete Raman signal from the whole fruit. However, handheld Raman spectrometers, which allow for quick scanning of samples with a handheld laser probe, can rapidly collect Raman spectra. Therefore, handheld Raman spectrometers are employed for the early detection of Huanglongbing in grapefruit. Based on the Raman spectra of standard substances, Sanchez et al. [92] observed that the intensity variation in Raman characteristic peaks of organic compounds in grapefruit is influenced by HLB. By developing an orthogonal partial least squares discriminant analysis (OPLS-DA) detection model, the detection accuracy of HLB reached 96.7%, surpassing that of the PCR method. A diagram of the Raman spectra and OPLS-DA model of grapefruit under different states is shown in Figure 12, while the Raman characteristic bands of grapefruit are listed in Table 7. Disease detection serves as the foundation for disease classification and provides a scientific basis for the management of plant diseases. Utilizing the Raman data of grapefruit, the research team developed an OPLS-DA model, which achieved 98% accuracy in distinguishing healthy grapefruit from HLB-infected grapefruit and 100% accuracy in differentiating early and late-stage HLB infections [93].
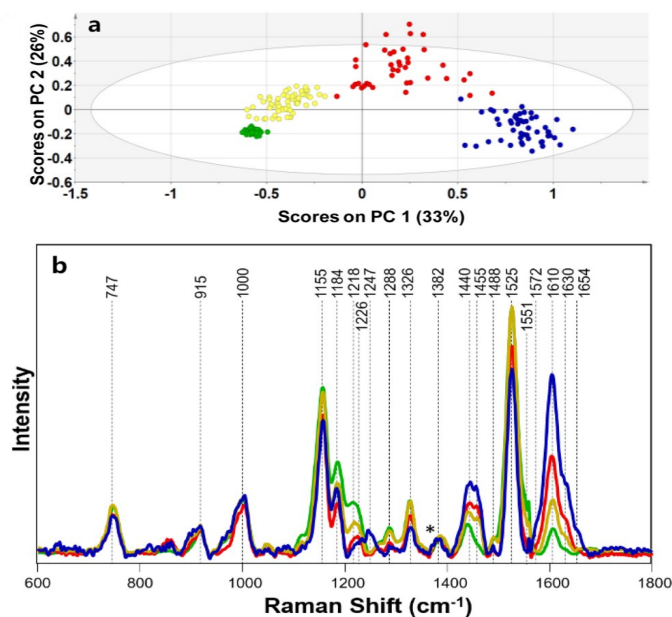

Figure 12. OPLS-DA (**a**) loadings plot and Raman spectra (**b**) of grapefruit leaves in greenhouse (green), in-feld 'healthy' (yellow), nutrient defcits (blue) and asymptomatic HLB infection (red). Spectra are normalized on the CH_2 vibrational band that is present in nearly all classes in biological molecules (marked by asterisks (*)).

4.1.3. Early Detection of Apple and Tomato Canker by Raman Spectroscopy

Apple canker, caused by Nectria galligena, results in wilting or even death of infected plant branches. This pathogen has a broad host range and infects various woody plants, such as peaches, cherries, and tomatoes, leading to a decrease in the yields of various fruits [94]. The early detection of canker disease helps prevent the spread of pathogenic conidia and improves fruit yield.

Due to the significant physiological and biochemical differences among various fruits, as well as the varying stages of disease progression, the detection of fruit diseases caused by the same pathogen in different samples presents a challenge. Raman spectroscopy can capture and identify biochemical information related to chemical bonds, molecular symmetry, and other parameters, enabling the early detection of fruit diseases caused by the same pathogen in different samples. Zhao et al. [66] applied PCA to extract spectral bands from data preprocessed by the air-PLS algorithm, with the scores of the first three principal components shown in Figure 13. The results indicated that the Least-Squares SVM model developed for the detection of apple canker achieved an accuracy of 89.33%. SERS improves the accuracy of early disease detection by amplifying the Raman signals. Fang et al. [95] employed SERS to detect apple canker disease and determined, through correlation analysis, that the air-PLS algorithm was the most effective preprocessing method, as shown in Figure 14. The characteristic Raman bands of the apples correspond to those in Table 7, with detection accuracies for BP-ANN, LS-SVM, and other models exceeding 90%. Raman spectroscopy is also applicable for classifying and detecting tomato canker disease caused by Nectria galligena. Perez et al. [96] collected Raman spectra from infected, asymptomatic, and healthy tomato plants, as shown in Figure 15, with the characteristic Raman bands for tomatoes aligning with those in Table 7. After spectral standardization preprocessing, a PCA-based LDA classification model was developed, achieving a classification accuracy of 97% for tomato canker disease.
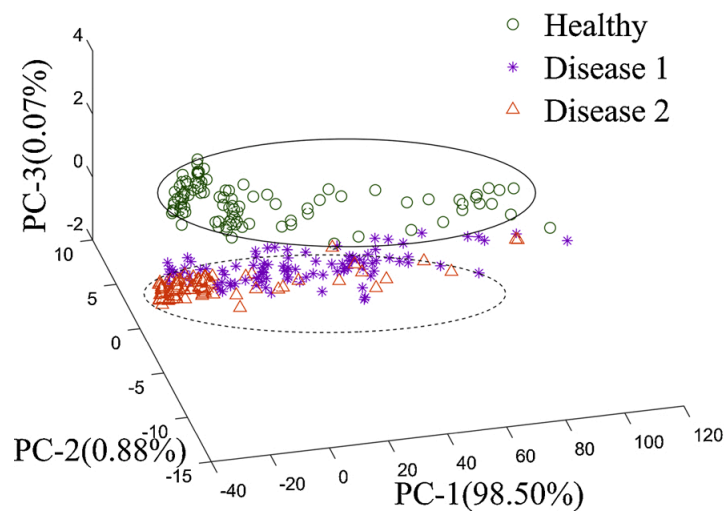

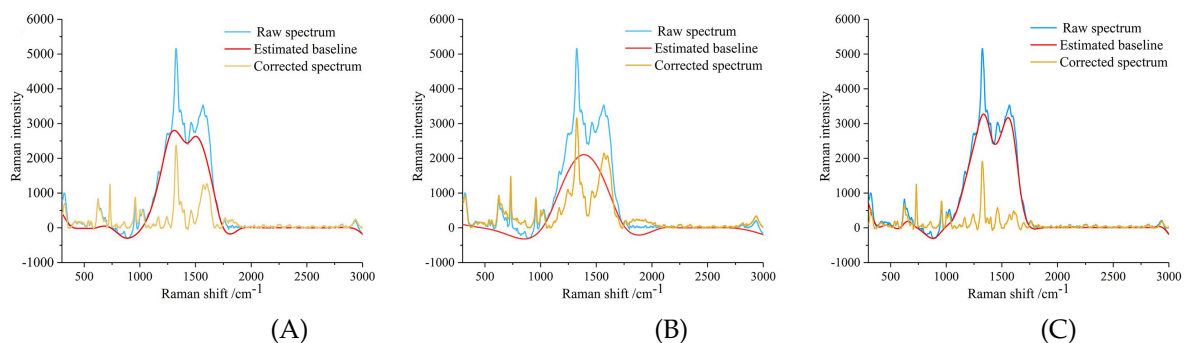**Figure 13.** Score plot of the spectral data of the first three PCs.

Figure 14. Spectral baseline correction: (**A**) using the MSBC algorithm for baseline correction, (**B**) using the AsLS algorithm for baseline correction, and (**C**) using the air-PLS algorithm for baseline correction. The blue line represents the original spectrum, the red line represents the estimated baseline, and the yellow line represents the corrected spectrum.
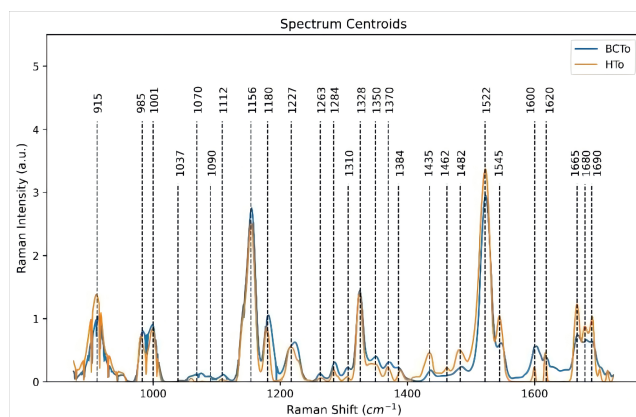
Figure 15. Raman spectra of asymptomatic tomato plants (BCTo) and healthy tomato plants (HTo).

Fruit diseases greatly affect both the yield and quality of fruits. Although Raman spectroscopy can identify early-stage fruit diseases, false negatives may arise due to the uneven distribution of pathogens within plants. Addressing the issue of false negatives in fruit disease detection can improve accuracy. In-depth research on fruit disease detection can be optimized by sample preprocessing, multi-technique detection methods, and enhanced equipment sensitivity [97,98].

Table 7. Vibrational bands and their assignments for some fruits.

Sample	Band (cm^{-1})	Vibrational Mode	Assignment
Grapefruit	747	γ(C−O−H) of COOH	Pectin [92]
	915	ν(C−O−C) in plane, symmetric	Cellulose, lignin [89]
	1000	ν_3(C−CH$_3$), phenylalanine	Carotenoids, protein [93]
	1155	asym ν(C−C) ring breathing	Carbohydrates, cellulose [92]
	1184	ν(C−O−H) next to aromatic ring+σ(CH)	Xylan [93]
	1247	(C−O) stretching (aromatic)	Lignin [89]
	1326	δ(CH$_2$)bending vibration	Cellulose, lignin [89]
	1440	δ(CH$_2$), δ(CH$_3$)	Aliphatic [99]
	1455	δCH$_2$ bending vibration	Aliphatic [99]
	1525–1551	ν(−C=C−) in plane	Carotenoids [93]
	1610	C=C−C ring	Lignin [99]
Citrus	1000-1008	ν(CH$_3$), δ(C−CH$_3$)	Carotenoids [80]
	1154–1157	ν(C−O−C), ν(C−C)	Carotenoids [85]
	1000–1008	ν(−C=C−) in plane	Carotenoids [80]
Apple	319	(C−C−C) or (C−O−C) skeletal bending	Cellulose [92]
	625	Skeletal bending	Lignin [93]
	731	Skeletal bending	Lignin [93]
	957	(C−C) or (C−O) stretching vibration	Cellulose [100]
	1165	(H−C−C) or (H−C−O) skeletal bending	Cellulose [93]
	1325	(C−H) bending vibration	Cellulose [100]
	1599	(C−C) aromatic ring	Lignin [66]
Tomato	915	ν(C−O−H) in plane, symmetric	Cellulose, lignin [96]
	985	δ(CH$_3$)	Chlorophylls [101]
	1001	δ(C−CH$_3$)	Carotenoids [102]
	1156	ν(C−C)	Carotenoids [102]
	1165	(H−C−C) or (H−C−O) skeletal bending	Cellulose [94]
	1180	ν(C−C), γ(CH)	Chlorophylls [103]
	1227	δ(CCH)	Cuticle triterpenoids [96]
	1328	δ(CH), ν(CN)	Chlorophylls, pyrrole ring [101]

Table 7. *Cont.*

Sample	Band (cm^{-1})	Vibrational Mode	Assignment
	1462	δ(CH$_2$), δ(CH$_3$)	Cuticle triterpenoids [102]
	1522	ν(C=C)	Carotenoids [102]
	1665	β sheet	Amide 1 [103]
	1690	β turn	Proteins [103]

Table 8. Vibrational bands and their assignments for some pesticides.

Sample	Calculation (cm^{-1})	SERS (cm^{-1})	Assignments
Thiabendazole	606	626	δ(C−C−C) , δ(S−C−N) [104]
	771	786	δ(C−H) [105]
	870	890	δ(C−C−C) , δ(C−H) [105]
	1010	1016	δ(C−H) [104]
	1401	1400	ν(C=C) [106]
	1584	1601	ν(C=N) [106]
	1641	1623	ν(C=N) [106]
Pyraclostrobin	778	780	δ C^{3}C^{11}O^{27}, ν C^{3}C^{11} [107]
	932	935	δ CNN rβ [107]
	1087	1092	ν_a N^{14}O^{15} / O^{22}C^{20} [107]
	1176	1174	δ CCH rγ, ν_s CC rγ [108]
	1367	1359	ω CH$_2$, ν_a C^{3}N^{33}C^{35} [108]
	1386	1388	ν C^{20}N^{14} [108]
	1598	1598	ν_s CC rγ [108]
Chlorpyrifos	605	606	P=S stretch [109]
	676	672	C–Cl stretch [109]
	1092	1096	P–O–C stretch [110]
	1572	1562	Ring stretching mode [110]
	1612	1600	C=C stretch [110]
Thiram	557	556	ν(S=S) [111]
	1147	1139	ρ(CH$_3$), ν(C-N) [111]
	1372	1379	δ_s(CH$_3$), ν(C-N) [112]
	1456	1444	ν(C-N), δ(CH$_3$), ρ(CH$_3$) [112]
	1498	1508	ρ(CH$_3$), ν(CN) [112]

Note : ν = stretching; γ = out-of-plane bending; ρ = rocking; ω = wagging; δ = bending; ν_a = antisymmetric stretching; ν_s = symmetric stretching; δ_s = symmetric bending; rβ, rγ = aromatic ring.

4.2. Application of Raman Spectroscopy in the Detection of Pesticide Residues in Fruits

Farmers use various pesticides to protect fruits from diseases and pests. However, the improper and excessive use of pesticides leads to the accumulation of multiple pesticide residues in the fruits [113]. In order to protect the health of consumers and improve the quality of agricultural products, it is necessary to detect pesticide residues in fruits with high precision. Due to its high sensitivity and strong Raman signal, SERS has been widely employed to detect pesticide residues in fruits. The effectiveness of SERS detection depends on the substrate utilized, and detection results can vary with different substrates [114].

4.2.1. Application of SERS Technique Based on AgNPs in Pesticide Residue Detection

Due to the high lipophilicity of pesticides, they penetrate the interior of fruits, making the detection of pesticide residues a challenge. The SERS technique enables the non-invasive detection of various analytes at trace levels, with silver nanometal materials commonly applied as SERS substrates for the detection of pesticide residues in fruits due to their strong electromagnetic field intensity effect resulting from plasma enhancement [115].

Molnar et al. [116] utilized the SERS technique based on nanosilver sol to detect residues of thiabendazole in blueberry extract. The results indicated that the lowest detection limit of pesticide residue after extract pretreatment was 0.09 µM. The raw and pretreated SERS spectra of the extract are shown in Figure 16. The substrate provides an adsorption surface that enhances the Raman signal, and AgNPs with various shapes offer differently shaped adsorption surfaces for molecules as SERS substrates to detect pesticide residues in fruits. Alfredo et al. [117] employed the SERS technique based on an AgNP ring to detect residues of the fungicide pyraclostrobin in lemons. The AgNP ring provided a larger adsorption surface for molecules, allowing the detection of the Raman signal, even when the concentration of pyraclostrobin was as low as 6×10^{-5} M. Table 9 summarizes the application of the SERS technique based on AgNPs in the detection of pesticide residues in fruits.

Table 9. Methods based on silver nanoparticles (Ag NPs) for the detection of pesticides in fruit.

| Matrix	Analytes	SERS Substrates	LOD	Reference
Apple	Thiram	Ag NPs	4.6261 ng/cm^2	[118]
	Thiabendazole, Acetamiprid, Phosmet	Polyurethane micelle/Ag NPs	0.02, 0.08, 0.1 µg/mL	[119]
	Chlorpyrifos	Ag NP	10 ng/ml	[120]
	Triphenyltin chloride	Ag NPs	6.25 ng/cm^2	[121]
	Thiabendazole	CNF-Ag NP	5 ppm	[122]
	Thiram	Ag NRs	1.0×10^{-9} g/cm^2	[123]
	Acetamiprid, Carbendazim, Chlorpyrifos	Ag NPs	5.4×10^{-3}, 1.4×10^{-2}, 6.4×10^{-2} ppm	[124]
	Metolcarb	Ag NPs	1.0×10^{-9} g/cm^2	[125]
	Thiabendazole, Thiram	Ag NPs	1.51×10^{-8}, 1.805×10^{-8} g/cm^2	[126]
	Thiram	Ag NPs	0.01 ppm	[127]
	Thiram	Ag NPs	5.313×10^{-10} g/cm^2	[128]
	Thiram	Ag NPs	2.88×10^{-8} g/cm^2	[129]
	Triazophos	Ag NPs	2.5×10^{-8} g/cm^2	[129]
	Triazophos	Ag NPs	2.5×10^{-8} M	[130]
	Thiram	Ag NPs	240 ng/cm^2	[131]
Citrus	Thiabendazole, Acetamiprid, Phosmet	Polyurethane micelle/Ag NPs	0.02, 0.08, 0.1 µg/mL	[119]
	Methy1 parathion	Ag NC@PE composite film	10 nM	[132]
	Thiabendazole	Ag NPs	4 ppm	[133]
	Thiram	Ag NPs	1.0×10^{-5} M	[134]
Grape	Thiram	Ag NPs	5.7061 ng/cm^2	[118]
	Thiram	Ag NPs	5.768×10^{-10} g/cm^2	[128]
Pear	Thiram	Ag NPs	5.1799 ng/cm^2	[118]
	Fenthion	Ag NPs	1.8×10^{-7} M	[135]
Cherry	Phosmet	Polyurethane-Ag NPs	0.6 µg/mL	[136]
	Thiabendazole, Acetamiprid, Phosmet	Polyurethane micelle/Ag NPs	0.02, 0.08, 0.1 µg/mL	[119]
	Triazophos, Methy1 parathion	Ag NPs	7.9×10^{-10}, 1.58×10^{-9} g/cm^2	[137]
Tomato	Chlorpyrifos	Ag colloid	1.0×10^{-9} mol/L	[138]
	Fenthion	Ag NPs	1.8×10^{-7} M	[135]
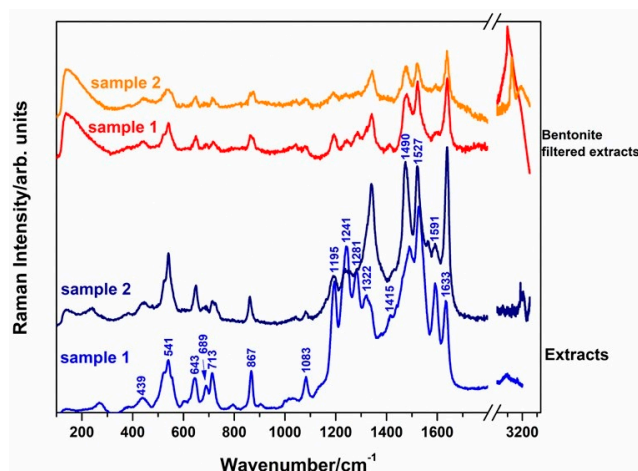
Figure 16. Original SERS spectra of two different blueberry extracts and SERS spectra after pretreatment.

4.2.2. Application of SERS Technique Based on AuNPs in Pesticide Residue Detection

The chemical properties of AgNPs are unstable and susceptible to oxidation and aggregation during storage and use, which diminishes the SERS signal. In contrast, the chemical properties of AuNPs are stable, largely unaffected by other substances in the system, and their surfaces are easily modified, enhancing the adsorption and detection of specific molecules. Therefore, AuNPs act as substrates for the SERS technique in detecting pesticide residues in fruits [25].

Xu et al. [139] utilized the SERS technique based on AuNPs to obtain the SERS spectrum of a chlorpyrifos standard solution. The theoretical and experimental spectra of the standard solution are shown in Figure 17, with the corresponding Raman characteristic bands detailed in Table 8. A strong linear relationship was demonstrated for chlorantraniliprole concentrations in citrus in the range of 3–20 mg/kg, with an R^2 value of 0.9979. The minimum detectable concentration was approximately 3 mg/kg. Combining gold nanoparticle structures with semiconductors or other materials facilitates charge transfer at interfaces, increasing the Raman scattering cross-section of molecules and enhancing the SERS effect. Xiao et al. [140] combined bacterial cellulose with AuNPs and employed the SERS technique based on this composite material to detect thiram residues in apples, achieving an R^2 of 0.99 and a detection limit of 0.98 ppm. Table 10 summarizes the application of the SERS technique based on AuNPs in the detection of pesticide residues in fruits.
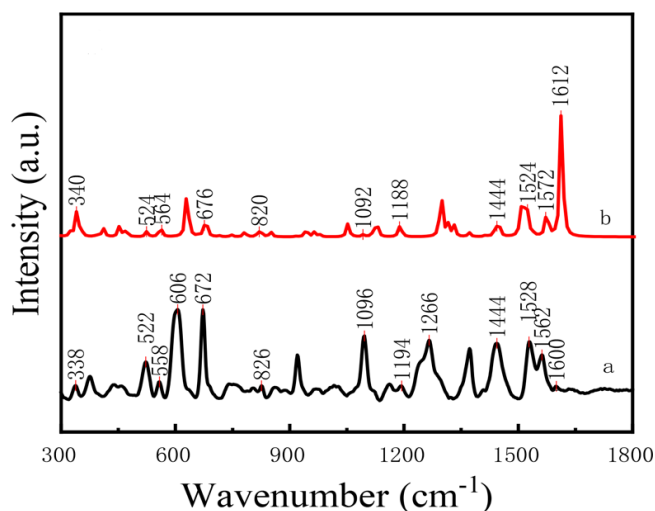

Figure 17. Spectrum of chlorpyrifos standard solution (**a**) and theoretical calculation spectrum (**b**).

Table 10. Methods based on gold nanoparticles (Au NPs) for the detection of pesticides in fruit.

Matrix	Analytes	SERS Substrates	LOD	Reference
Apple	Methy1 parathion	Au NPs	0.011 μg/cm^2	[141]
	Phosmet	Au NPs	0.5 mg/kg	[142]
	Methy1 parathion, triazophos, phosmet	Snowflake-like Au NPs	0.026, 0.031, 0.032 ng/cm^2	[143]
	Imidacloprid	Au NPs	0.02 mg/kg	[144]
	Methy1 parathion	Au NPs@tape	26.3 ng/cm^2	[145]
	Phosmet	Au NPs	0.5 μg/g	[146]
	Thiram	Au NRs	0.24 ng/cm^2	[147]
	Methy1 parathion	Au NRs	110–440 ng/cm^2	[148]
	Thiram	bipyramid AuNPs	36.58 ng/cm^2	[149]
	Thiabendazole	Au NRs	0.06 mg/kg	[150]
	Acephate, Cypermethrin, Tsumacide	Au NPs	1×10^{-12}, 1×10^{-6}, 1×10^{-13} g/cm^2	[135]
	Carbaryl, Cypermethrin, Permethrin, Phosmet	Au NPs-ZrO2 NFs	1×10^{-7}, 1×10^{-6}, 1×10^{-7}, 1×10^{-8} M	[151]
	Carbaryl, Methy1 parathion	Au NPs	2.5×10^{-9}, 5.2×10^{-6} M	[152]
	Chlorpyrifos, Omethoate	Au NPs	2.64×10^{-6}, 1.63×10^{-6} g/cm^2	[153]
	Methy1 parathion	Au NPs	3.658×10^{-8} g/cm^2	[149]
	Paraoxon	Au NPs	1×10^{-8} M	[154]
	Phosmet, Thiram	Au NPs	0.1, 0.1 ppm	[155]
	Phosmet, Triazophos	Au NPs	0.2, 0.2 ppm	[156]
	Thiabendazole	Au–Pt–Pd	0.5 ppm	[157]
	Thiabendazole, Thiram	Au NRs	7.9×10^{-10}, 7.6×10^{-10} g/cm^2	[158]
	Thiram	Au NPs	4.62×10^{-3} ppm	[159]
	Thiram	Au NPs	1.0×10^{-9} M	[160]
	Thiram	Au NPs	5.0×10^{-9} g/cm^2	[161]
Citrus	Methy1 parathion	Au NPs@tape	26.3 ng/cm^2	[145]
	Thiabendazole	Au NP-based UF membrane	0.125 μg/g	[162]
Grape	Carbaryl, Methy1 parathion	Au NPs	2.5×10^{-9}, 5.2×10^{-6} M	[152]
Pear	Chlorpyrifos	Au NP	0.35 mg/kg	[163]
	Acephate	Au NFs	5.4×10^{-12} M	[137]
	Thiabendazole, Thiram	Au NRs	8×10^{-10}, 4.1×10^{-11} g/cm^2	[158]
	Thiram	Au NPs	4.62×10^{-3} ppmM	[159]
	Thiram	Au NPs	1×10^{-9} M	[160]
Tomato	Thiram	bipyramid AuNPs	31.56 ng/cm^2	[149]
	Carbendazol, Parathion	Au NPs-microhemisphere PDMS NFs	1×10^{-8}, 1×10^{-8} M	[164]
	Methy1 parathion	Au NPs	3.156×10^{-8} g/cm^2	[149]
	Thiabendazole, Thiram	Au NRs	4.7×10^{-11}, 2.9×10^{-11} g/cm^2	[158]
Lemon	Thiram	Au NPs and SiNWP	72 ng/cm^2	[165]
Strawberry	Thiram	AuNPs	5.0×10^2 ppm	[166]

4.2.3. Application of SERS Technique Based on Gold and Silver Mixed Nanoparticles in Pesticide Residue Detection

Ionic gold and silver in chloroauric acid or silver nitrate can be chemically reduced to their elemental state. However, the morphology and size of monometallic nanoparticle materials influence their optical absorption and SERS characteristics. Furthermore, in multicomponent nanomaterials, there is a synergistic effect between different components, collectively enhancing the SERS signal [167]. Therefore, gold-silver alloy nanoparticles can serve as SERS substrates to detect pesticide residues in fruits [168].

Asgari et al. [169] employed the SERS technique based on Au@Ag nanoparticles to detect residues of thiabendazole and other pesticides in strawberries. The Raman spectra of four pesticide residues are shown in Figure 18. PLS and PCA models were

established for the preprocessed spectra, and Raman peaks were distinctly observable, even at low pesticide concentrations of 5 μg/kg. In contrast, Rizzato et al. [170] utilized the SERS technique based on AgNPs to detect thiabendazole residue in strawberries, with a minimum detection limit of 500 μg/kg. Thiabendazole, used to control fungal diseases in crops, is also required in apple cultivation. Yan et al. [171] applied the SERS technique based on Au@Ag nanoparticles to detect thiabendazole residue in apples and found that the SERS activity was optimal when the silver shell thickness was 7.3 nm, with a minimum detection limit of 5 ng/cm^2. Similarly, Dayalan et al. [172] applied the SERS technique with gold core-silver shell nanoparticles to detect thiabendazole residue on apple peels. The results indicated that substrate intensity was optimal at a pH of 5, with the lowest detection limit of 0.1 ng/cm^2, as shown in Figure 19. Table 11 summarizes the application of the SERS technique based on Au@Ag in the detection of pesticide residues in fruits.

Table 11. Methods based on the combination of gold and silver nanoparticles (Au@Ag NPs) for the detection of pesticides in fruit.

| Matrix	Analytes	SERS Substrates	LOD	Reference
Apple	Thiram	Au@Ag NRs	7.5×10^{-8} M	[172]
	Thiram	Au@Ag NPs	1.5×10^{-2} ppm	[173]
	Thiram	Au@Ag on ZnO nanosheets	2.0×10^{-10} g/cm^2	[174]
Grape	Difenoconazole	Au@Ag NPs	2.8×10^{-8} M	[175]
Pear	Flusilazole	Au@Ag NPs	<0.1 μg/g	[176]
Tomato	Thiram	u@Ag on ZnO nanosheets	2.0×10^{-10} g/cm^2	[177]
Peach	Methy1 parathion, Triazophos	Au@Ag NPs	1.0×10^{-3}, 1.0×10^{-3} ppm	[177]
	Thiacloprid, Profenofos, Oxamy1	Au@Ag NPs	0.1, 0.01, 0.01 mg/kg	[178]
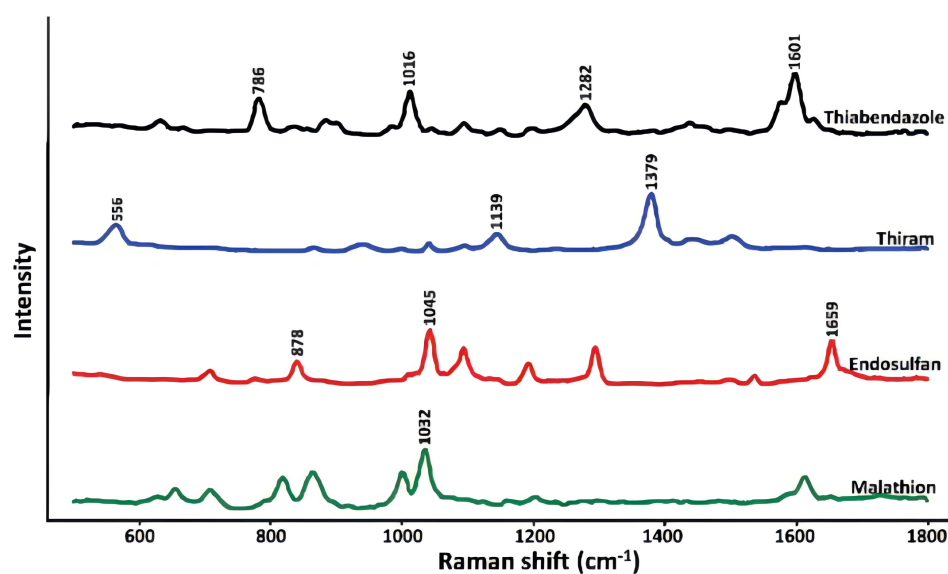
Figure 18. Raman spectra of four pesticides.

Raman spectroscopy is used to detect pesticide residues in fruits; however, it is limited in its ability to uniformly detect multiple pesticide residues within the same sample. To address this limitation, enzyme inhibition methods can be employed to mask interference from other pesticides, or luminescent labeling methods can be used to tag specific pesticides.

These methods are then combined with Raman spectral detection to enhance pesticide residue detection [179,180].
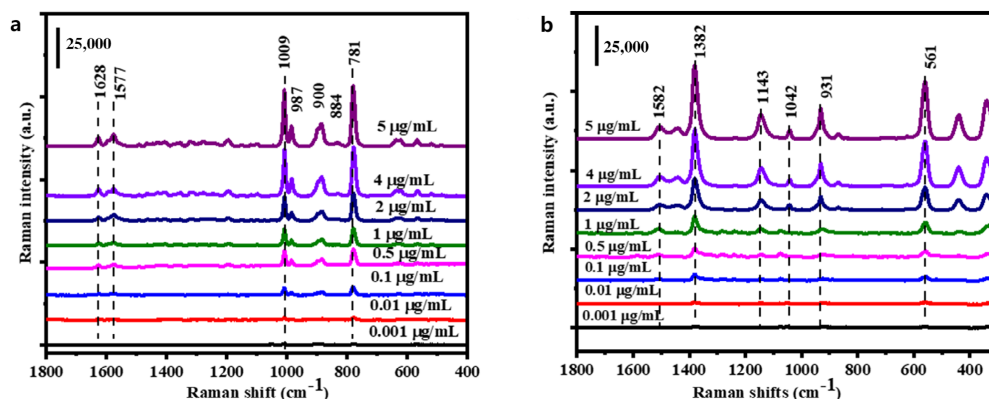

Figure 19. SERS spectra of (**a**) Tbz and (**b**) thiram in standard solutions with different concentrations (pH = 5).

4.3. Application of Raman Spectroscopy in Fruit Origin Identification

Many regions produce the same type of fruit, but fruits from different regions can differ significantly in terms of their nutritional composition, taste, and size. Fruit origin traceability technology helps protect well-known local specialties and ensures the authenticity of the food market [181]. A sufficient number of spectra from different points in samples (such as the top, middle, and bottom) should be collected and preprocessed. This method can obtain the average spectra of multiple sampling points, which reduces the impact of local variations on the overall detection results and improves the stability of the spectral data. Therefore, Raman spectroscopy is applied to identify the origin of fruits [182].

In the field of fruit origin identification, traditional methods cannot non-destructively analyze the biochemical information inside the fruit. In contrast, Raman spectroscopy can non-destructively acquire internal information for fruit origin identification [114]. Lu et al. [183] found that after SG and MSC preprocessing, the Long Short-Term Memory (LSTM) network model for cherry origin identification achieved the highest accuracy, with an average recognition accuracy of 99.12%. SVM can also serve as an identification model for cherry origin. This team combined SG and MSC spectral preprocessing algorithms with variance feature screening algorithms to establish a GA-SVM discrimination model, concluding that both models achieved 100% accuracy in identifying cherry origin [184]. SERS can also be utilized for fruit origin identification due to its strong Raman signal. Traksele et al. [185] applied the SERS technique based on silver nanosol to classify the origin of bilberries in Northern Europe. The average SERS spectra of bilberries from each country are shown in Figure 20. The results were consistent with those obtained by high-performance liquid chromatography, confirming the applicability of the SERS-PCA method for determining bilberry origin.

Raman spectroscopy can determine the origin of fruit by analyzing the differences in the chemical compounds between samples. However, establishing an accurate identification model requires a large number of representative sample data, and the generalization ability of the model is often limited. To improve identification accuracy, intelligent and automated equipment is utilized in the origin identification process, improving both the speed and precision of identification [186,187].
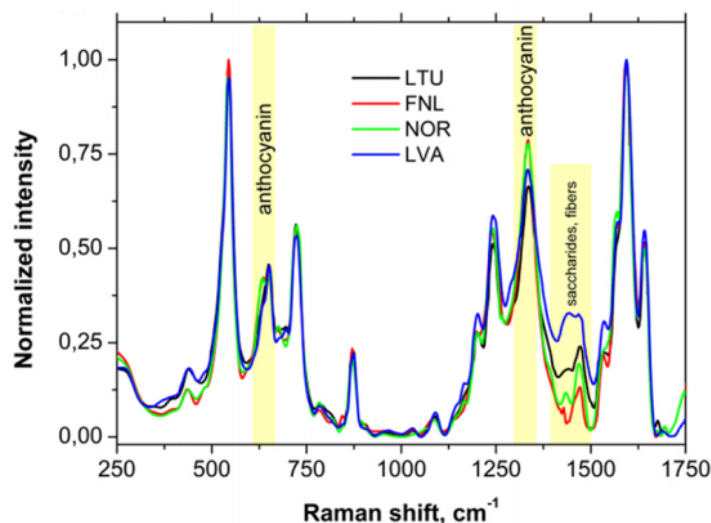
Figure 20. Average SERS spectra of bilberry in each country.

5. Prospects and Challenges

Raman spectroscopy has been systematically applied in the field of fruit quality detection, characterized by its rapid, accurate, and non-destructive nature. However, traditional Raman spectroscopy faces several challenges, such as weak Raman signals, the inability to detect information in the interior of samples, and susceptibility to fluorescence background interference. Advanced spectral techniques, such as SERS, CM-RS, and SORS, have been gradually introduced. Combining these techniques with machine learning algorithms enables more efficient applications in areas such as agricultural product quality detection, biomedical identification, and environmental monitoring.

Raman spectroscopy offers many advantages but still faces several challenges, such as difficulties in multicomponent analysis and quantitative analysis, as well as the need for specific sample pretreatment processes. With advancements in computer technology and chemometrics, computational power has significantly improved, enabling the faster and more efficient processing and analysis of large Raman spectral datasets. Progress in chemometrics has also provided advanced tools for Raman data analysis, allowing the extraction of information from the interior of samples and improving the accuracy and reliability of detection. For samples requiring specific pretreatment, appropriate preparation can be made based on the physicochemical properties of the sample, such as slicing, dilution, or freeze-drying. For high-density solids or powder samples, grinding or compaction can create a uniform surface, whereas for high-concentration liquid samples, dilution can reduce the background signal from Raman scattering. It is believed that Raman spectroscopy will be widely applied in food safety detection, materials science, life sciences, environmental monitoring, and other research fields, particularly in fruit quality detection, with a brighter application prospect. It will also extend to various interdisciplinary fields, fully leveraging its unique advantages.

References

1. Jaeger, S.R.; Antúnez, L.; Ares, G. An exploration of what freshness in fruit means to consumers. *Food Res. Int.* **2023**, *165*, 112491. [CrossRef]
2. Wu, J.P.; Huang, G.W.; LI, J. Research status and prospect of visual and spectral detection technology for fruit diseases. *Chin. J. Agric. Mach. Chem.* **2023**, *44*, 112–118.
3. de Andrade, J.P.; Galvan, D.; Kato, L.S.; Conte-Junior, C.A. Consumption of fruits and vegetables contaminated with pesticide residues in Brazil: A systematic review with health risk assessment. *Chemosphere* **2023**, *322*, 138244. [CrossRef] [PubMed]
4. Hidalgo, M.J.; Gaiad, J.E.; Goicoechea, H.C.; Mendoza, A.; Pérez-Rodríguez, M.; Pellerano, R.G. Geographical origin identification of mandarin fruits by analyzing fingerprint signatures based on multielemental composition. *Food Chem. X* **2023**, *20*, 101040. [CrossRef] [PubMed]
5. Zhao, M.; You, Z.; Chen, H.; Wang, X.; Ying, Y.; Wang, Y. Integrated Fruit Ripeness Assessment System Based on an Artificial Olfactory Sensor and Deep Learning. *Foods* **2024**, *13*, 793. [CrossRef]
6. Zhang, H.; Cao, L.; Brodsky, J.; Gablech, I.; Xu, F.; Li, Z.; Korabecna, M.; Neuzil, P. Quantitative or digital PCR? A comparative analysis for choosing the optimal one for biosensing applications. *TrAC Trends Anal. Chem.* **2024**, *174*, 117676. [CrossRef]
7. Ma, N.; Zhu, J.; Wang, H.; Qian, M.C.; Xiao, Z. Comparative Investigation of Aroma-Active Volatiles in ("Ruixue","Liangzhi","Crystal Fuji," and "Guifei") Apples by Application of Gas Chromatography–Mass Spectrometry–Olfactometry (GC–MS–O) and Two-Dimensional Gas Chromatography-Quadrupole Mass Spectrometry (GC × GC-qMS) Coupled with Sensory Molecular Science. *J. Agric. Food Chem.* **2024**, *72*, 25229–25250. [PubMed]
8. Fakhlaei, R.; Babadi, A.A.; Sun, C.; Ariffin, N.M.; Khatib, A.; Selamat, J.; Xiaobo, Z. Application, challenges and future prospects of recent nondestructive techniques based on the electromagnetic spectrum in food quality and safety. *Food Chem.* **2024**, *441*, 138042. [CrossRef] [PubMed]
9. Yu, Y.; Zhang, J.; Wang, L.; Ni, Z.; Lu, J.; Gao, L. Hot-carrier engineering for two-dimensional integrated infrared optoelectronics. *InfoMat* **2024**, *6*, e12556. [CrossRef]
10. Orlando, A.; Franceschini, F.; Muscas, C.; Pidkova, S.; Bartoli, M.; Rovere, M.; Tagliaferro, A. A comprehensive review on Raman spectroscopy applications. *Chemosensors* **2021**, *9*, 262. [CrossRef]
11. Lu, L.; Wang, Y.; Liang, C.; Fan, J.; Su, X.; Huang, M. A Novel Distributed Optical Fiber Temperature Sensor Based on Raman anti-Stokes Scattering Light. *Appl. Sci.* **2023**, *13*, 11214. [CrossRef]
12. Qing, B.L.; Lan, Y.M. Soliton resonances and soliton molecules of pump wave and Stokes wave for a transient stimulated Raman scattering system in optics. *Eur. Phys. J. Plus* **2022**, *137*, 1227.
13. Saletnik, A.; Saletnik, B.; Puchalski, C. Overview of popular techniques of Raman spectroscopy and their potential in the study of plant tissues. *Molecules* **2021**, *26*, 1537. [CrossRef] [PubMed]
14. Zhao, M.; Wu, B.; Liu, J.; Lei, L. Anti-Stokes/Stokes temperature calibration and its application in laser-heating diamond anvil cells. *Chin. Phys. B* **2023**, *32*, 090704. [CrossRef]
15. Kolesov, B.A. Hydrogen bonds: Raman spectroscopic study. *Int. J. Mol. Sci.* **2021**, *22*, 5380. [CrossRef] [PubMed]
16. FeNg, X.; ZhaNg, Q.; Zhu, Z. Rapid classification of citrus fruits based on Raman spectroscopy and pattern recognition techniques. *Food Sci. Technol. Res.* **2013**, *19*, 1077–1084. [CrossRef]
17. Lee, K.S.; Landry, Z.; Pereira, F.C.; Wagner, M.; Berry, D.; Huang, W.E.; Taylor, G.T.; Kneipp, J.; Popp. J.; Stocker, R.; et al. Raman microspectroscopy for microbiology. *Nat. Rev. Methods Prim.* **2021**, *1*, 80. [CrossRef]
18. Lin, S.; Cheng, Z.; Li, Q.; Wang, R.; Yu, F. Toward sensitive and reliable surface-enhanced Raman scattering imaging: From rational design to biomedical applications. *ACS Sensors* **2021**, *6*, 3912–3932. [CrossRef] [PubMed]
19. Silge, A.; Weber, K.; Cialla-May, D.; Müller-Bötticher, L.; Fischer, D.; Popp, J. Trends in pharmaceutical analysis and quality control by modern Raman spectroscopic techniques. *TrAC Trends Anal. Chem.* **2022**, *153*, 116623. [CrossRef]
20. Wang, L.; Tang, J.W.; Li, F.; Usman, M.; Wu, C.Y.; Liu, Q.H.; Kang, H.Q.; Liu, W.; Gu, B. Identification of bacterial pathogens at genus and species levels through combination of Raman spectrometry and deep-learning algorithms. *Food Microbiol. Spectr.* **2022**, *10*, e02580-22. [CrossRef]
21. Qu, C.; Li, Y.; Du, S.; Geng, Y.; Su, M.; Liu, H. Raman spectroscopy for rapid fingerprint analysis of meat quality and security: Principles, progress and prospects. *Food Res. Int.* **2022**, *161*, 111805. [CrossRef] [PubMed]
22. He, Q.F.; Zhang, Y.J.; Yang, Z.L.; Dong, J.C.; Lin, X.M.; Li, J.F. Surface-Enhanced Raman Spectroscopy: Principles, Methods, and Applications in Energy Systems. *Chin. J. Chem.* **2023**, *41*, 355–369. [CrossRef]
23. Liu, C.; Xu, D.; Dong, X.; Huang, Q. A review: Research progress of SERS-based sensors for agricultural applications. *Trends Food Sci. Technol.* **2022**, *128*, 90–101. [CrossRef]
24. Jones, T. Fabrication of nanostructured electrodes for electrochemical surface-enhanced Raman spectroscopy (E-SERS): A review. *Mater. Sci. Technol.* **2023**, *39*, 2287–2301. [CrossRef]
25. Lin, D.Y.; Yu, C.Y.; Ku, C.A.; Chung, C.K. Design, fabrication, and applications of SERS substrates for food safety detection. *Micromachines* **2023**, *14*, 1343. [CrossRef]

26. Du, M.; Sun, Z.; Xie, M.; Gu, S.; Chen, Y.; Wang, Q. A new method for rapid identification of traditional Chinese medicine based on a new silver sol: Using the SERS spectrum for quality control of flavonoids and flavonoid glycosides in Potentilla discolor Bge. *J. Mater. Chem. C* **2023**, *11*, 15138–15148. [CrossRef]

27. Ye, Y.; Wang, J.; Fang, Z.; Yan, Y.; Geng, Y. Periodic Folded Gold Nanostructures with a Sub-10 nm Nanogap for Surface-Enhanced Raman Spectroscopy. *ACS Appl. Mater. Interfaces* **2024**, *16*, 10450–10458. [CrossRef] [PubMed]

28. Zhang, L.; Weng, Y.J.; Liu, X.; Gu, W.; Zhang, X.; Han, L. Fe (III) mixed IP6@ Au NPs with enhanced SERS activity for detection of 4-ATP. *Sci. Rep.* **2020**, *10*, 5752. [CrossRef]

29. Pham, A.T.; Bui, H.N.; Mai, Q.D.; Le, A.T. Flexible, high-performance and facile PVA/cellulose/Ag SERS chips for in-situ and rapid detection of thiram pesticide in apple juice. *Heliyon* **2023**, *9*, e19926. [CrossRef] [PubMed]

30. Odetade, D.F.; Rickard, J.J.S.; Bai, H.; Goldberg Oppenheimer, P. Development and Optimization of Micro-Nanotopographical Platforms for Surface Enhanced Raman Scattering Biomolecular Detection. *Adv. Mater. Interfaces* **2024**, *2024*, 2400352. [CrossRef]

31. Liu, D.; Zheng, Y.; Chen, L.; Wen, D. Prevalence of small-sized microplastics in coastal sediments detected by multipoint confocal micro-Raman spectrum scanning. *Sci. Total. Environ.* **2021**, *831*, 154741. [CrossRef] [PubMed]

32. Olivier, A.; Artur, A.; Aurélien, T. Confocal Raman microscope with versatile dual polarization snapshot acquisition. *Opt. Express* **2022**, *30*, 46734–46748.

33. Nicolson, F.; Kircher, M.F.; Stone, N.; Matousek, P. Spatially offset Raman spectroscopy. *Nat. Rev. Methods Prim.* **2021**, *50*, 556–568.

34. Vardaki, M.Z.; Schulze, H.G.; Serrano, K.; Blades, M.W.; Devine, D.V.; Turner, R.F. Assessing the quality of stored red blood cells using handheld Spatially Offset Raman spectroscopy with multisource correlation analysis. *Spectrochim. Acta Part A Mol. Biomol. Spectrosc.* **2022**, *276*, 121220. [CrossRef]

35. Berry, M.E.; McCabe, S.M.; Sloan-Dennison, S.; Laing, S.; Shand, N.C.; Graham, D.; Faulds, K. Tomographic imaging and localization of nanoparticles in tissue using surface-enhanced spatially offset raman spectroscopy. *ACS Appl. Mater. Interfaces* **2022**, *14*, 31613–31624. [CrossRef]

36. Shillito, G.E.; McMillan, L.; Bruce, G.D.; Dholakia, K. To focus-match or not to focus-match inverse spatially offset Raman spectroscopy: A question of light penetration. *Opt. Express* **2022**, *30*, 8876–8888. [CrossRef] [PubMed]

37. Razzell Hollis, J.; Sharma, S.; Abbey, W.; Bhartia, R.; Beegle, L.; Fries, M.; Hein, J.D.; Monacelli, B.; Nordman, A.D. A deep ultraviolet Raman and fluorescence spectral library of 51 organic compounds for the SHERLOC instrument onboard Mars 2020. *Astrobiology* **2023**, *23*, 1–23. [CrossRef]

38. Ardini, B.; Bassi, A.; Candeo, A.; Genco, A.; Trovatello, C.; Liu, F.; Zhu, X.; Valentini, G.; Cerullo, G.; Manzoni, C.; et al. High-throughput multimodal wide-field Fourier-transform Raman microscope. *Optica* **2023**, *10*, 663–670. [CrossRef]

39. Petreanu, I.; Niculescu, V.C.; Enache, S.; Iacob, C.; Teodorescu, M. Structural characterization of silica and amino-silica nanoparticles by Fourier transform infrared (FTIR) and raman spectroscopy. *Anal. Lett.* **2023**, *56*, 390–403. [CrossRef]

40. Bailo, E.; Deckert, V. Tip-enhanced Raman scattering. *Chem. Soc. Rev.* **2024**, *37*, 921–930. [CrossRef] [PubMed]

41. Cai, Z.F.; Kumar, N.; Zenobi, R. Probing On-Surface Chemistry at the Nanoscale Using Tip-Enhanced Raman Spectroscopy. *CCS Chem.* **2023**, *5*, 55–71. [CrossRef]

42. Ferrara, M.A.; Ranjan, R.; Righini, G.C.; Sirleto, L. Stimulated Raman scattering: Towards applications in nano and biophotonics. In *Advances in Nonlinear Photonics*; Righini, G.C., Sirleto, L., Eds.; Woodhead Publishing: London, UK, 2023; pp. 489–515.

43. Brzozowski, K.; Matuszyk, E.; Pieczara, A.; Firlej, J.; Nowakowska, A.M.; Baranska, M. Stimulated Raman scattering microscopy in chemistry and life science–development, innovation, perspectives. *Biotechnol. Adv.* **2022**, *60*, 108003. [CrossRef]

44. Weng, S.; Yuan, H.; Zhang, X.; Li, P.; Zheng, L.; Zhao, J.; Huang, L. Deep learning networks for the recognition and quantitation of surface-enhanced Raman spectroscopy. *Analyst* **2020**, *145*, 4827–4835. [CrossRef] [PubMed]

45. Fang, S.; Wu, S.; Chen, Z.; He, C.; Lin, L.; Ye, J. Recent progress and applications of Raman spectrum denoising algorithms in chemical and biological analyses: A review. *TrAC Trends Anal. Chem.* **2024**, *172*, 4117578. [CrossRef]

46. Mostafapour, S.; Dörfer, T.; Heinke, R.; Rösch, P.; Popp, J.; Bocklitz, T. Investigating the effect of different pre-treatment methods on Raman spectra recorded with different excitation wavelengths. *Spectrochim. Acta Part A Mol. Biomol. Spectrosc.* **2023**, *302*, 123100. [CrossRef]

47. Mosca, S.; Sowoidnich, K.; Mehta, M.; Skinner, W.H.; Gardner, B.; Palombo, F.; Stone, N.; Matousek, P. 10 kHz Shifted-Excitation Raman Difference Spectroscopy with Charge-Shifting Charge-Coupled Device Read-Out for Effective Mitigation of Dynamic Interfering Backgrounds. *Appl. Spectrosc.* **2023**, *77*, 569–582. [CrossRef] [PubMed]

48. Oksenberg, E.; Shlesinger, I.; Tek, G.; Koenderink, A.F.; Garnett, E.C. Complementary Surface-Enhanced Raman Scattering (SERS) and IR Absorption Spectroscopy (SEIRAS) with Nanorods-on-a-Mirror. *Adv. Funct. Mater.* **2023**, *8*, 2211154. [CrossRef]

49. Sharan, T.S.; Sharma, S.; Sharma, N. Denoising and spike removal from Raman spectra using double density dual-tree complex wavelet transform. *J. Appl. Spectrosc.* **2021**, *88*, 117–124. [CrossRef]

50. A, M.A.; V, K. The estimation of signal in time domain analysis with a mean smoothening, gaussian smoothening and median filter. *J. Crit. Rev.* **2020**, *7*, 1180–1183.

51. Guo, Y.; Jin, W.; Wang, W.; He, Y.; Qiu, S. Baseline correction for Raman spectra using a spectral estimation-based asymmetrically reweighted penalized least squares method. *Appl. Opt.* **2023**, *62*, 4766–4776. [CrossRef]

52. Atiogbe, A.H.; Benjamin, A.; Alfred, O. Raman spectra recovery using a second derivative technique and range independent baseline correction algorithm. *OSA Contin.* **2021**, *4*, 2468–2480.

53. Sheehy, G.; Picot, F.; Dallaire, F.; Ember, K.; Nguyen, T.; Petrecca, K.; Trudel, D.; Leblond, F. Open-sourced Raman spectroscopy data processing package implementing a baseline removal algorithm validated from multiple datasets acquired in human tissue and biofluids. *J. Biomed. Opt.* **2023**, *28*, 025002. [CrossRef]

54. Wang, P.; Zhan, K.; Wang, X.; Peng, Y.; Liu, S. Comparison of NIR and Raman spectrometries as quantitative methods to monitor polyethylene content in recycled polypropylene. *Polym. Test.* **2023**, *119*, 107938. [CrossRef]

55. Mooij, B.J.; Schmidt, R.W.; Vijvers, W.A.; Ariese, F. A versatile Raman setup with time-gating and fast wide-field imaging capabilities. *Spectrochim. Acta Part A Mol. Biomol. Spectrosc.* **2024**, *318*, 124388. [CrossRef]

56. Menghrajani, K.; Mingzhou, C.; Dholakia, K.; Barnes, W. Probing vibrational strong coupling of molecules with Wavelength-modulated Raman spectroscopy (dataset). *Adv. Opt. Mater.* **2022**, *10*, 2102065. [CrossRef]

57. Tian, L.; Jiang, H.; Zhang, X. A rapid and non-destructive identification for paper cup evidence based on shifted-excitation Raman difference spectroscopy and SOM clustering. *J. Forensic Sci.* **2024**, *69*, 81–93. [CrossRef] [PubMed]

58. Ye, J.; Ma, X.; Zhang, Y.; Xu, J.; Zhang, H.; Yao, T.; Leng, J.; Zhou, P. Revealing the dynamics of intensity fluctuation transfer in a random Raman fiber laser. *Photonics Res.* **2022**, *10*, 618–627. [CrossRef]

59. Lin, L.; He, H.; Xue, R.; Zhang, Y.; Wang, Z.; Nie, S.; Ye, J. Direct and quantitative assessments of near-infrared light attenuation and spectroscopic detection depth in biological tissues using surface-enhanced Raman scattering. *Med-X* **2023**, *1*, 9. [CrossRef]

60. Pan, L.; Pipitsunthonsan, P.; Daengngam, C.; Channumsin, S.; Sreesawet, S.; Chongcheawchamnan, M. Method for classifying a noisy Raman spectrum based on a wavelet transform and a deep neural network. *IEEE Access* **2020**, *8*, 202716–202727. [CrossRef]

61. Wei, C.; Zhang, X.; Xu, L.; Ding, F.; Yang, E. Overall recursive least squares and overall stochastic gradient algorithms and their convergence for feedback nonlinear controlled autoregressive systems. *Int. J. Robust Nonlinear Control.* **2022**, *32*, 5534–5554. [CrossRef]

62. Yuan, N.Z.; Chen, S.H.; Mu, T.T. Research on plastic classification based on Raman spectroscopy combined with deep learning algorithm. *Opt. Instrum.* **2023**, *45*, 35–43.

63. Chen, X.; Fan, Y.; Ma, Z.; Tan, S.; Li, N.; Song, X.; Huang, Y.; Zhang, J.; Zhang, W. Feature Extraction of Oil–Paper Insulation Raman Spectroscopy Based on Manifold Dimension Transformation. *Appl. Sci.* **2023**, *13*, 7626. [CrossRef]

64. Ni, X.; Jiang, Y.; Zhang, Y.; Zhou, Y.; Zhao, Y.; Guo, F.; Wang, H. Identification of liquid milk adulteration using Raman spectroscopy combined with lactose indexed screening and support vector machine. *Int. Dairy J.* **2023**, *146*, 105751. [CrossRef]

65. Abdul, R.; Abhishek, D.B. PCA based feature extraction and MPSO based feature selection for gene expression microarray medical data classification. *Meas. Sensors* **2024**, *31*, 100945.

66. Zhao, Y.; Fang, S.; Ye, Y.; Yu, K. Chemometric development using portable molecular vibrational spectrometers for rapid evaluation of AVC (Valsa mali Miyabe et Yamada) infection of apple trees. *Vib. Spectrosc.* **2021**, *114*, 103231. [CrossRef]

67. Pulpito, O.; Acito, N.; Diani, M.; Ferri, G.; Grasso, R.; Zissis, D. Saliency-Aided Online RPCA for Moving Target Detection in Infrared Maritime Scenarios. *Sensors* **2023**, *23*, 6334. [CrossRef]

68. Jiang, K.; Song, Y.; Li, S.; Chen, K. Feature extraction and recognition of face image based on 2DPCA with LDA algorithm. *IEEE* **2024**, *7*, 1861–1866.

69. Wu, S.; Chen, J.; Li, L.; Zhang, C.; Huang, R.; Zhang, Q. Quantitative Inversion of Lunar Surface Chemistry Based on Hyperspectral Feature Bands and Extremely Randomized Trees Algorithm. *Remote Sens.* **2022**, *14*, 5248. [CrossRef]

70. Chen, Z.H.; Gu, J.; Chen, W.H.; Mo, L.N.; Q, H.L. SPA algorithm based on double latent variable technology is applied to NIR wavelength screening. *Spectrosc. Spectr. Anal.* **2018**, *S1*, 111–112.

71. Qin, G.; Zhang, A.; Chen, F.; Man, H.; Liu, H.; Li, M.; Jia, Z. Identification of appetite suppressants through Fourier transform infrared spectroscopy and filtered spectral feature extraction. *Microchem. J.* **2024**, *197*, 109843. [CrossRef]

72. Camp, C.H., Jr. Raman signal extraction from CARS spectra using a learned-matrix representation of the discrete Hilbert transform. *Opt. Express* **2022**, *30*, 26057–26071. [CrossRef]

73. Malavi, D.; Nikkhah, A.; Alighaleh, P.; Einafshar, S.; Raes, K.; Van Haute, S. Detection of saffron adulteration with Crocus sativus style using NIR-hyperspectral imaging and chemometrics. *Food Control* **2024**, *157*, 110189. [CrossRef]

74. Boginskaya, I.; Safiullin, R.; Tikhomirova, V.; Kryukova, O.; Nechaeva, N.; Bulaeva, N.; Golukhova, E.; Ryzhikov, I.; Kost, O.; Kurochkin, I.; et al. Human Angiotensin I-Converting Enzyme Produced by Different Cells: Classification of the SERS Spectra with Linear Discriminant Analysis. *Biomedicines* **2022**, *10*, 1389. [CrossRef]

75. Liang, H.; Tai, S. VLSI test through an improved LDA classification algorithm for test cost reduction. *Microelectron. J.* **2022**, *125*, 105461.

76. Zhang, P.; Liu, B.; Mu, X.; Xu, J.; Du, B.; Wang, J.; Liu, Z.; Tong, Z. Performance of Classification Models of Toxins Based on Raman Spectroscopy Using Machine Learning Algorithms. *Molecules* **2023**, *29*, 197. [CrossRef]

77. Majid, A.; Hamid, U. Optimizing feature selection methods by removing irrelevant features using sparse least squares. *Expert Syst. Appl.s* **2022**, *200*, 116928.

78. Atin, R.; Subrata, C. Support vector machine in structural reliability analysis: A review. *Reliab. Eng. Syst. Saf.* **2023**, *233*, 109126.

79. Yuan, D.; Wang, X. Improved SVM Algorithm Financial Management Model for Data Mining. *J. Inf. Knowl. Manag.* **2024**, *23*, 2450020. [CrossRef]

80. Cai, J.; Zou, C.; Yin, L.; Jiang, S.; El-Seedi, H.R.; Guo, Z. Characterization and recognition of citrus fruit spoilage fungi using Raman scattering spectroscopic imaging. *Vib. Spectrosc.* **2023**, *124*, 103474. [CrossRef]

81. Henry, P.M.; Dilla-Ermita, C.J.; Goldman, P.; Jaime, J.; Ramos, G. Sporodochia formed by *Fusarium oxysporum* f. sp. fragariae produce airborne conidia and are ubiquitous on diseased strawberry plants in California. *Phytopathology* **2023**, *113*, 1399–1404. [CrossRef]

82. Zhou, C. The status of citrus Huanglongbing in China. *Trop. Plant Pathol.* **2020**, *45*, 279–284. [CrossRef]

83. Minas, I.S.; Blanco-Cipollone, F.; Sterle, D. Accurate non-destructive prediction of peach fruit internal quality and physiological maturity with a single scan using near infrared spectroscopy. *Food Chem.* **2021**, *335*, 127626. [CrossRef] [PubMed]

84. Morán, F.; Herrero-Cervera, M.; Carvajal-Rojas, S.; Marco-Noales, E. Real-time on-site detection of the three 'Candidatus Liberibacter'species associated with HLB disease: A rapid and validated method. *Front. Plant Sci.* **2023**, *14*, 1176513. [CrossRef]

85. Kong, L.; Liu, T.; Qiu, H.; Yu, X.; Wang, X.; Huang, Z.; Huang, M. Early diagnosis of citrus Huanglongbing by Raman spectroscopy and machine learning. *Laser Phys. Lett.* **2023**, *21*, 015701. [CrossRef]

86. Dai, F.; Qiu, Z.Y.; Qiu, Q.; Liu, C.J.; Huang, G.Z.; Huang, Y.L.; Deng, X.L. Rapid detection method of citrus huanglongbing based on Raman spectroscopy and autofluorescence spectroscopy. *Intell. Agric.* **2019**, *1*, 10.

87. Liu, Y.; Xiao, H.; Hao, Y.; Ye, L.; Jiang, X.; Wang, H.; Sun, X. Diagnosis of citrus greening using raman spectroscopy-based pattern recognition. *J. Appl. Spectrosc.* **2020**, *87*, 150–158. [CrossRef]

88. Wang, K.; Liao, Y.; Meng, Y.; Jiao, X.; Huang, W.; Liu, T.C.Y. The early, rapid, and non-destructive detection of citrus Huanglongbing (HLB) based on microscopic confocal Raman. *Food Anal. Methods* **2019**, *12*, 2500–2508. [CrossRef]

89. Sanchez, L.; Pant, S.; Irey, M.; Mandadi, K.; Kurouski, D. Detection and identification of canker and blight on orange trees using a hand-held Raman spectrometer. *J. Raman Spectrosc.* **2019**, *50*, 1875–1880. [CrossRef]

90. Pérez, M.R.V.; Mendoza, M.G.G.; Elías, M.G.R.; González, F.J.; Contreras, H.R.N.; Servín, C.C. Raman spectroscopy an option for the early detection of citrus Huanglongbing. *Appl. Spectrosc.* **2016**, *70*, 829–839. [CrossRef] [PubMed]

91. Ferguson, K.; da Cruz, M.A.; Ferrarezi, R.; Dorado, C.; Bai, J.; Cameron, R.G. Impact of Huanglongbing (HLB) on grapefruit pectin yield and quality during grapefruit maturation. *Food Hydrocoll.* **2021**, *113*, 106553. [CrossRef]

92. Sanchez, L.; Pant, S.; Mandadi, K.; Kurouski, D. Raman spectroscopy vs quantitative polymerase chain reaction in early stage Huanglongbing diagnostics. *Sci. Rep.* **2020**, *10*, 10101. [CrossRef] [PubMed]

93. Sanchez, L.; Pant, S.; Xing, Z.; Mandadi, K.; Kurouski, D. Rapid and noninvasive diagnostics of Huanglongbing and nutrient deficits on citrus trees with a handheld Raman spectrometer. *Anal. Bioanal. Chem.* **2019**, *411*, 3125–3133. [CrossRef]

94. Feng, H.; Wang, C.; He, Y.; Tang, L.; Han, P.; Liang, J.; Huang, L. Apple Valsa canker: Insights into pathogenesis and disease control. *Phytopathol. Res.* **2023**, *5*, 45. [CrossRef]

95. Fang, S.; Zhao, Y.; Wang, Y.; Li, J.; Zhu, F.; Yu, K. Surface-enhanced Raman scattering spectroscopy combined with chemical imaging analysis for detecting apple Valsa canker at an early stage. *Front. Plant Sci.* **2022**, *13*, 802761. [CrossRef]

96. Vallejo-Pérez, M.R.; Sosa-Herrera, J.A.; Navarro-Contreras, H.R.; Álvarez-Preciado, L.G.; Rodríguez-Vázquez, Á.G.; Lara-Ávila, J.P. Raman spectroscopy and machine-learning for early detection of bacterial canker of tomato: The asymptomatic disease condition. *Plants* **2021**, *10*, 1542. [CrossRef]

97. Wang, K.; Li, Z.; Li, J.; Lin, H. Raman spectroscopic techniques for nondestructive analysis of agri-foods: A state-of-the-art review. *Trends Food Sci. Technol.* **2021**, *118*, 490–504. [CrossRef]

98. Guo, Z.; Wang, M.; Barimah, A.O.; Chen, Q.; Li, H.; Shi, J.; Zou, X. Label-free surface enhanced Raman scattering spectroscopy for discrimination and detection of dominant apple spoilage fungus. *Int. J. Food Microbiol.* **2021**, *338*, 108990. [CrossRef] [PubMed]

99. Weng, S.; Hu, X.; Wang, J.; Tang, L.; Li, P.; Zheng, S.; Zhang, L.; Huang, L.; Xin, Z. Advanced application of Raman spectroscopy and surface-enhanced Raman spectroscopy in plant disease diagnostics: A review. *J. Agric. Food Chem.* **2021**, *69*, 2950–2964. [CrossRef]

100. Li, D.; Zhu, Z.; Sun, D.W. Visualization of the in situ distribution of contents and hydrogen bonding states of cellular level water in apple tissues by confocal Raman microscopy. *Analyst* **2020**, *145*, 897–907. [CrossRef]

101. Campos, M.T.; Maia, L.F.; Dos Santos, H.F.; Edwards, H.G.; Oliveira, L.F. Revealing the chemical synergism in coloring tomatoes by Raman spectroscopy. *J. Raman Spectrosc.* **2023**, *54*, 1314–1326. [CrossRef]

102. Akpolat, H.; Barineau, M.; Jackson, K.A.; Akpolat, M.Z.; Francis, D.M.; Chen, Y.J.; Rodriguez-Saona, L.E. High-throughput phenotyping approach for screening major carotenoids of tomato by handheld raman spectroscopy using chemometric methods. *Sensors* **2020**, *20*, 3723. [CrossRef]

103. Mandrile, L.; Rotunno, S.; Miozzi, L.; Vaira, A.M.; Giovannozzi, A.M.; Rossi, A.M.; Noris, E. Nondestructive Raman spectroscopy as a tool for early detection and discrimination of the infection of tomato plants by two economically important viruses. *Anal. Chem.* **2019**, *91*, 9025–9031. [CrossRef] [PubMed]

104. Brezestean, I.A.; Tosa, N.; Falamas, A.; Cuibus, D.; Muntean, C.M.; Bende, A.; Cozar, B.; Berghian-Grosan, C.; Farcău, C. Silver nanoparticle films obtained by convective self-assembly for surface-enhanced Raman spectroscopy analyses of the pesticides thiabendazole and endosulfan. *Front. Chem.* **2022**, *10*, 915337. [CrossRef] [PubMed]

105. Nie, P.; Dong, T.; Xiao, S.; Lin, L.; He, Y.; Qu, F. Quantitative determination of thiabendazole in soil extracts by surface-enhanced Raman spectroscopy. *Molecules* **2018**, *23*, 1949. [CrossRef] [PubMed]

106. Lin, L.; Dong, T.; Nie, P.; Qu, F.; He, Y.; Chu, B.; Xiao, S. Rapid determination of thiabendazole pesticides in rape by surface enhanced Raman spectroscopy. *Sensors* **2018**, *18*, 1082. [CrossRef] [PubMed]

107. Dominguez, A.N.; Emmert, G.E.; Gil, D.M.; Alvarez, R.M.S. Experimental and theoretical vibrational study of the fungicide pyraclostrobin. *Spectrochim. Acta Part A Mol. Biomol. Spectrosc.* **2021**, *259*, 119888. [CrossRef]

108. Serin, S. Computational insights into E/Z isomerism of fluoxastrobin, an antifungal agent: A DFT/TD-DFT study. *J. Mol. Struct.* **2023**, *1287*, 135713. [CrossRef]

109. Zhu, X.; Li, W.; Wu, R.; Liu, P.; Hu, X.; Xu, L.; Xiong, Z.; Wen, Y.; Ai, S. Rapid detection of chlorpyrifos pesticide residue in tea using surface-enhanced Raman spectroscopy combined with chemometrics. *Spectrochim. Acta Part A Mol. Biomol. Spectrosc.* **2021**, *250*, 119366. [CrossRef] [PubMed]

110. Chen, Z.; Dong, X.; Liu, C.; Wang, S.; Dong, S.; Huang, Q. Rapid detection of residual chlorpyrifos and pyrimethanil on fruit surface by surface-enhanced Raman spectroscopy integrated with deep learning approach. *Sci. Rep.* **2023**, *13*, 18955. [CrossRef] [PubMed]

111. Zhai, W.; Cao, M.; Xiao, Z.; Li, D.; Wang, M. Rapid detection of malathion, phoxim and thiram on orange surfaces using Ag nanoparticle modified PDMS as surface-enhanced Raman spectroscopy substrate. *Foods* **2022**, *11*, 3579. [CrossRef]

112. Dao, T.C.; Luong, T.Q.N.; Cao, T.A.; Kieu, N.M. High-sensitive SERS detection of thiram with silver nanodendrites substrate. *Adv. Nat. Sci. Nanosci. Nanotechnol.* **2019**, *10*, 025012. [CrossRef]

113. El-Sheikh, E.S.A.; Ramadan, M.M.; El-Sobki, A.E.; Shalaby, A.A.; McCoy, M.R.; Hamed, I.A.; Ashour, M.B.; Hammock, B.D. Pesticide residues in vegetables and fruits from farmer markets and associated dietary risks. *Molecules* **2022**, *27*, 8072. [CrossRef]

114. Yan, Z.; Nie, J.; Cheng, Y.; Han, L.; Farooq, S. Method development, validation, and risk assessment of multiple pesticide residues of fruits in China. *Environ. Sci. Pollut. Res.* **2024**, *31*, 18826–18841. [CrossRef]

115. Zhao, H.; Li, W.; Li, J.; Sun, Y.; Yang, Q.; Sun, M. Advances of SERS applications in clinic samples analysis. *Appl. Spectrosc. Rev.* **2024**, *59*, 157–186. [CrossRef]

116. Müller Molnár, C.; Berghian-Groșan, C.; Măgdaș, D.A.; Cîntă Pînzaru, S. Surface-Enhance Raman Spectroscopy Detection of Thiabendazole in Frozen Food Products: The Case of Blueberries and Their Extracts. *Chemosensors* **2023**, *11*, 505. [CrossRef]

117. Dominguez, A.N.; Jimenez, L.E.; Álvarez, R.M.S. Rapid detection of pyraclostrobin fungicide residues in lemon with surface-enhanced Raman spectroscopy. *J. Food Meas. Charact.* **2023**, *17*, 6350–6362. [CrossRef]

118. Wang, K.; Huang, M.; Chen, J.; Lin, L.; Kong, L.; Liu, X.; Wang, H.; Lin, M. A "drop-wipe-test" SERS method for rapid detection of pesticide residues in fruits. *J. Raman Spectrosc.* **2018**, *49*, 493–498. [CrossRef]

119. Kang, Y.; Li, L.; Chen, W.; Zhang, F.; Du, Y.; Wu, T. Rapid in situ SERS analysis of pesticide residues on plant surfaces based on micelle extraction of targets and stabilization of Ag nanoparticle aggregates. *Food Anal. Methods* **2018**, *11*, 3161–3169. [CrossRef]

120. Tang, J.; Chen, W.; Ju, H. Rapid detection of pesticide residues using a silver nanoparticles coated glass bead as nonplanar substrate for SERS sensing. *Sensors Actuators B Chem.* **2019**, *287*, 576–583. [CrossRef]

121. Jiang, J.; Gao, J.M.; Guo, J.S.; Zhou, Q.H.; Liu, X.H.; Ouyang, W.J.; Zhang, P.; Fu, W.L.; Zhang, W.; He, S.X. Identification and analysis of triphenyltin chloride with surface enhanced Raman scattering spectroscopy. *Chemosphere* **2016**, *161*, 96–103. [CrossRef] [PubMed]

122. Liou, P.; Nayigiziki, F.X.; Kong, F.; Mustapha, A.; Lin, M. Cellulose nanofibers coated with silver nanoparticles as a SERS platform for detection of pesticides in apples. *Carbohydr. Polym.* **2017**, *157*, 643–650. [CrossRef]

123. Kumar, S.; Goel, P.; Singh, J.P. Flexible and robust SERS active substrates for conformal rapid detection of pesticide residues from fruits. *Sensors Actuators B Chem.* **2017**, *241*, 577–583. [CrossRef]

124. Zhai, C.; Peng, Y.; Li, Y.; Chao, K. Extraction and identification of mixed pesticides' Raman signal and establishment of their prediction models. *J. Raman Spectrosc.* **2017**, *48*, 494–500. [CrossRef]

125. Wang, Y.; Wang, M.; Sun, X.; Shi, G.; Ma, W.; Ren, L. Rapid, simple and quantitative detection of metolcarb residues in apples by surface-enhanced Raman scattering. *AIP Adv.* **2018**, *8*, 075001. [CrossRef]

126. Zong, C.; Ge, M.; Pan, H.; Wang, J.; Nie, X.; Zhang, Q.; Zhao, W.; Liu, X.; Yu, Y. In situ synthesis of low-cost and large-scale flexible metal nanoparticle–polymer composite films as highly sensitive SERS substrates for surface trace analysis. *RSC Adv.* **2019**, *9*, 2857–2864. [CrossRef] [PubMed]

127. D'Agostino, A.; Giovannozzi, A.M.; Mandrile, L.; Sacco, A.; Rossi, A.M.; Taglietti, A. In situ seed-growth synthesis of silver nanoplates on glass for the detection of food contaminants by surface enhanced Raman scattering. *Talanta* **2020**, *216*, 120936. [CrossRef]

128. Sun, L.; Wang, C. Highly sensitive and rapid surface enhanced Raman spectroscopic (SERS) determination of thiram on the epidermis of fruits and vegetables using a silver nanoparticle-modified fibrous swab. *Anal. Lett.* **2020**, *53*, 973–983. [CrossRef]

129. Gong, X.; Tang, M.; Gong, Z.; Qiu, Z.; Wang, D.; Fan, M. Screening pesticide residues on fruit peels using portable Raman spectrometer combined with adhesive tape sampling. *Food Chem.* **2019**, *295*, 254–258. [CrossRef]

130. Shao, F.; Cao, J.; Ying, Y.; Liu, Y.; Wang, D.; Guo, X.; Wu, Y.; Wen, Y.; Yang, H. Preparation of hydrophobic film by electrospinning for rapid SERS detection of trace triazophos. *Sensors* **2020**, *20*, 4120. [CrossRef]

131. Dai, H.; Sun, Y.; Ni, P.; Lu, W.; Jiang, S.; Wang, Y.; Li, Z.; Li, Z. Three-dimensional TiO2 supported silver nanoparticles as sensitive and UV-cleanable substrate for surface enhanced Raman scattering. *Sensors Actuators B Chem.* **2017**, *242*, 260–268. [CrossRef]

132. Zhou, N.; Meng, G.; Huang, Z.; Ke, Y.; Zhou, Q.; Hu, X. A flexible transparent Ag-NC@ PE film as a cut-and-paste SERS substrate for rapid in situ detection of organic pollutants. *Analyst* **2016**, *141*, 5864–5869. [CrossRef]

133. Feng, J.; Hu, Y.; Grant, E.; Lu, X. Determination of thiabendazole in orange juice using an MISPE-SERS chemosensor. *Food Chem.* **2018**, *239*, 816–822. [CrossRef] [PubMed]

134. Alyami, A.; Quinn, A.J.; Iacopino, D. Flexible and transparent Surface Enhanced Raman Scattering (SERS)-Active Ag NPs/PDMS composites for in-situ detection of food contaminants. *Talanta* **2019**, *201*, 58–64. [CrossRef]

135. Wang, M.; Shi, G.; Zhu, Y.; Wang, Y.; Ma, W. Au-decorated dragonfly wing bioscaffold arrays as flexible surface-enhanced Raman scattering (SERS) substrate for simultaneous determination of pesticide residues. *Nanomaterials* **2018**, *8*, 289. [CrossRef]

136. Kang, Y.; Wu, T.; Chen, W.; Li, L.; Du, Y. A novel metastable state nanoparticle-enhanced Raman spectroscopy coupled with thin layer chromatography for determination of multiple pesticides. *Food Chem.* **2019**, *270*, 494–501. [CrossRef]

137. Shi, G.; Wang, M.; Zhu, Y.; Wang, Y.; Ma, W. Synthesis of flexible and stable SERS substrate based on Au nanofilms/cicada wing array for rapid detection of pesticide residues. *Opt. Commun.* **2018**, *425*, 49–57. [CrossRef]

138. Ma, P.; Wang, L.; Xu, L.; Li, J.; Zhang, X.; Chen, H. Rapid quantitative determination of chlorpyrifos pesticide residues in tomatoes by surface-enhanced Raman spectroscopy. *Eur. Food Res. Technol.* **2020**, *246*, 239–251. [CrossRef]

139. Wang, X.; Ai, S.; Xiong, A.; Zhou, W.; He, L.; Teng, J.; Geng, X.; Wu, R. SERS combined with QuEChERS using NBC and Fe3O4 MNPs as cleanup agents to rapidly and reliably detect chlorpyrifos pesticide in citrus. *Anal. Methods* **2023**, *15*, 6266–6274. [CrossRef] [PubMed]

140. Xiao, L.; Feng, S.; Hua, M.Z.; Lu, X. Rapid determination of thiram on apple using a flexible bacterial cellulose-based SERS substrate. *Talanta* **2023**, *254*, 124128. [CrossRef] [PubMed]

141. Xie, J.; Li, L.; Khan, I.M.; Wang, Z.; Ma, X. Flexible paper-based SERS substrate strategy for rapid detection of methyl parathion on the surface of fruit. *Spectrochim. Acta Part A Mol. Biomol. Spectrosc.* **2020**, *231*, 118104. [CrossRef]

142. Jiang, L.; Gu, K.; Liu, R.; Jin, S.; Wang, H.; Pan, C. Rapid detection of pesticide residues in fruits by surface-enhanced Raman scattering based on modified QuEChERS pretreatment method with portable Raman instrument. *SN Appl. Sci.* **2019**, *1*, 1–9. [CrossRef]

143. Huang, D.; Zhao, J.; Wang, M.; Zhu, S. Snowflake-like gold nanoparticles as SERS substrates for the sensitive detection of organophosphorus pesticide residues. *Food Control* **2020**, *108*, 106835. [CrossRef]

144. Hou, R.; Pang, S.; He, L. In situ SERS detection of multi-class insecticides on plant surfaces. *Anal. Methods* **2015**, *7*, 6325–6330. [CrossRef]

145. Chen, J.; Huang, Y.; Kannan, P.; Zhang, L.; Lin, Z.; Zhang, J.; Chen, T.; Guo, L. Flexible and adhesive surface enhance Raman scattering active tape for rapid detection of pesticide residues in fruits and vegetables. *Anal. Chem.* **2016**, *88*, 2149–2155. [CrossRef] [PubMed]

146. Luo, H.; Huang, Y.; Lai, K.; Rasco, B.A.; Fan, Y. Surface-enhanced Raman spectroscopy coupled with gold nanoparticles for rapid detection of phosmet and thiabendazole residues in apples. *Food Control* **2016**, *68*, 229–235. [CrossRef]

147. Zhu, J.; Liu, M.J.; Li, J.J.; Li, X.; Zhao, J.W. Multi-branched gold nanostars with fractal structure for SERS detection of the pesticide thiram. *Spectrochim. Acta Part A Mol. Biomol. Spectrosc.* **2018**, *189*, 586–593. [CrossRef]

148. Wu, H.; Luo, Y.; Hou, C.; Huo, D.; Wang, W.; Zhao, J.; Lei, Y. Rapid and fingerprinted monitoring of pesticide methyl parathion on the surface of fruits/leaves as well as in surface water enabled by gold nanorods based casting-and-sensing SERS platform. *Talanta* **2019**, *200*, 84–90. [CrossRef] [PubMed]

149. Wu, H.; Luo, Y.; Hou, C.; Huo, D.; Zhou, Y.; Zou, S.; Zhao, J.; Lei, Y. Flexible bipyramid-AuNPs based SERS tape sensing strategy for detecting methyl parathion on vegetable and fruit surface. *Sensors Actuators B Chem.* **2019**, *285*, 123–128. [CrossRef]

150. Fu, G.; Sun, D.W.; Pu, H.; Wei, Q. Fabrication of gold nanorods for SERS detection of thiabendazole in apple. *Talanta* **2019**, *195*, 841–849. [CrossRef]

151. Lee, H.; Liao, J.D.; Sivashanmugan, K.; Liu, B.H.; Fu, W.E.; Chen, C.C.; Chen, G.D; Juang, Y.D. Gold nanoparticle-coated ZrO2-nanofiber surface as a SERS-active substrate for trace detection of pesticide residue. *Nanomaterials* **2018**, *8*, 402. [CrossRef]

152. Lin, S.; Li, X.; Fang, G.; Zhao, H.; Wang, L.; Dong, B. Tetragonal superlattice of elongated rhombic dodecahedra for sensitive SERS determination of pesticide residues in fruit. *ACS Appl. Mater. Interfaces* **2020**, *12*, 56350–56360. [CrossRef]

153. Chen, J.; Dong, D.; Ye, S. Detection of pesticide residue distribution on fruit surfaces using surface-enhanced Raman spectroscopy imaging. *RSC Adv.* **2018**, *8*, 4726–4730. [CrossRef]

154. Tran, M.; Fallatah, A.; Whale, A.; Padalkar, S. Utilization of inexpensive carbon-based substrates as platforms for sensing. *Sensors* **2018**, *18*, 2444. [CrossRef]

155. Dowgiallo, A.M.; Guenther, D.A. Determination of the limit of detection of multiple pesticides utilizing gold nanoparticles and surface-enhanced Raman spectroscopy. *J. Agric. Food Chem.* **2019**, *67*, 12642–12651. [CrossRef] [PubMed]

156. Zhang, H.; Sun, L.; Zhang, Y.; Kang, Y.; Hu, H.; Tang, H.; Du, Y. Production of stable and sensitive SERS substrate based on commercialized porous material of silanized support. *Talanta* **2017**, *174*, 301–306. [CrossRef]

157. Chang, F.C.; Huang, J.W.; Chen, C.H. Au–Pt–Pd spherically self-assembled nano-sieves as SERS sensors. *J. Alloy. Compd.* **2020**, *843*, 155885. [CrossRef]

158. Hu, B.; Sun, D.W.; Pu, H.; Wei, Q. Rapid nondestructive detection of mixed pesticides residues on fruit surface using SERS combined with self-modeling mixture analysis method. *Talanta* **2020**, *217*, 120998. [CrossRef]

159. Kong, L.; Huang, M.; Chen, J.; Lin, M. In situ detection of thiram in fruits and vegetables by colorimetry/surface-enhanced Raman spectroscopy. *Laser Phys.* **2020**, *30*, 065602. [CrossRef]

160. Yu, F.; Su, M.; Tian, L.; Wang, H.; Liu, H. Organic solvent as internal standards for quantitative and high-throughput liquid interfacial SERS analysis in complex media. *Anal. Chem.* **2018**, *90*, 5232–5238. [CrossRef] [PubMed]

161. Ouyang, L.; Dai, P.; Yao, L.; Zhou, Q.; Tang, H.; Zhu, L. A functional Au array SERS chip for the fast inspection of pesticides in conjunction with surface extraction and coordination transferring. *Analyst* **2019**, *144*, 5528–5537. [CrossRef] [PubMed]

162. Hong, J.; Kawashima, A.; Hamada, N. A simple fabrication of plasmonic surface-enhanced Raman scattering (SERS) substrate for pesticide analysis via the immobilization of gold nanoparticles on UF membrane. *Appl. Surf. Sci.e* **2017**, *407*, 440–446. [CrossRef]

163. Xu, Q.; Guo, X.; Xu, L.; Ying, Y.; Wu, Y.; Wen, Y.; Yang, H. Template-free synthesis of SERS-active gold nanopopcorn for rapid detection of chlorpyrifos residues. *Sensors Actuators B Chem.* **2017**, *241*, 1008–1013. [CrossRef]

164. Zhang, L.; Li, X.; Liu, W.; Hao, R.; Jia, H.; Dai, Y.; Amin, M.; You, H.; Li, T.; Fang, J. Highly active Au NP microarray films for direct SERS detection. *J. Mater. Chem. C* **2019**, *7*, 15259–15268. [CrossRef]

165. Cui, H.; Li, S.; Deng, S.; Chen, H.; Wang, C. Flexible, transparent, and free-standing silicon nanowire SERS platform for in situ food inspection. *ACS Sensors* **2017**, *2*, 386–393. [CrossRef]

166. Chen, M.; Luo, W.; Liu, Q.; Hao, N.; Zhu, Y.; Liu, M.; Wang, L.; Yang, H.; Chen, X. Simultaneous in situ extraction and fabrication of surface-enhanced Raman scattering substrate for reliable detection of thiram residue. *Anal. Chem.* **2018**, *99*, 13647–13654. [CrossRef]

167. Zhao, Z.; Huang, Y.; Fan, Y.; Lai, K. Rapid detection of flusilazole in pears with Au@ Ag nanoparticles for surface-enhanced Raman scattering. *Nanomaterials* **2018**, *8*, 94. [CrossRef] [PubMed]

168. Liu, K.; Bai, Y.; Zhang, L.; Yang, Z.; Fan, Q.; Zheng, H.; Yin, Y.; Gao, C. Porous Au–Ag nanospheres with high-density and highly accessible hotspots for SERS analysis. *Nano Lett.* **2016**, *16*, 3675–3681. [CrossRef] [PubMed]

169. Asgari, S.; Wu, G.; Aghvami, S.A.; Zhang, Y.; Lin, M. Optimisation using the finite element method of a filter-based microfluidic SERS sensor for detection of multiple pesticides in strawberry. *Food Addit. Contam. Part A* **2021**, *38*, 646–658. [CrossRef] [PubMed]

170. Rizzato, M.L.; Picone, A.L.; Romano, R.M. A facile method for in-situ detection of thiabendazole residues in fruit and vegetable peels using Surface-Enhanced Raman Spectroscopy. *Talanta Open* **2023**, *7*, 10023. [CrossRef]

171. Li, X.; Zhang, Y.; Awais, M.; Zhang, H.; Naqvi, S.M.Z.A.; Li, L.; Xiong, Y.; Hu, J. Analysis and experimental assessment of an optimized SERS substrate used to detect thiabendazole in apples with high sensitivity. *Anal. Bioanal. Chem.* **2024**, *416*, 497–508. [CrossRef] [PubMed]

172. Dayalan, S.; Sudewi, S.; Zulfajri, M.; Kao, C.L.; Huang, G.G. Effect of pH on the optimization of cysteine-functionalized gold core-silver shell nanoparticles for surface-enhanced Raman scattering-based pesticide detection on apple peels. *J. Chin. Chem. Soc.* **2023**, *70*, 1821–1834. [CrossRef]

173. Pu, H.; Huang, Z.; Xu, F.; Sun, D.W. Two-dimensional self-assembled Au-Ag core-shell nanorods nanoarray for sensitive detection of thiram in apple using surface-enhanced Raman spectroscopy. *Food Chem.* **2021**, *343*, 128548. [CrossRef]

174. Hussain, N.; Pu, H.; Hussain, A.; Sun, D.W. Rapid detection of ziram residues in apple and pear fruits by SERS based on octanethiol functionalized bimetallic core-shell nanoparticles. *Spectrochim. Acta Part A Mol. Biomol. Spectrosc.* **2020**, *236*, 118357. [CrossRef]

175. Wang, K.; Sun, D.W.; Pu, H.; Wei, Q. Shell thickness-dependent Au@ Ag nanoparticles aggregates for high-performance SERS applications. *Talanta* **2019**, *195*, 506–515. [CrossRef] [PubMed]

176. Wang, K.; Sun, D.W.; Pu, H.; Wei, Q. Surface-enhanced Raman scattering of core-shell Au@ Ag nanoparticles aggregates for rapid detection of difenoconazole in grapes. *Talanta* **2019**, *191*, 449–456. [CrossRef]

177. Yaseen, T.; Pu, H.; Sun, D.W. Rapid detection of multiple organophosphorus pesticides (triazophos and parathion-methyl) residues in peach by SERS based on core-shell bimetallic Au@ Ag NPs. *Food Addit. Contam. Part A* **2019**, *36*, 762–778. [CrossRef]

178. Yaseen, T.; Pu, H.; Sun, D.W. Fabrication of silver-coated gold nanoparticles to simultaneously detect multi-class insecticide residues in peach with SERS technique. *Talanta* **2019**, *196*, 537–545. [CrossRef]

179. Zhang, D.; Liang, P.; Chen, W.; Tang, Z.; Li, C.; Xiao, K.; Jin, S.; Ni, D.; Yu, Z. Rapid field trace detection of pesticide residue in food based on surface-enhanced Raman spectroscopy. *Microchim. Acta* **2021**, *188*, 1–28. [CrossRef]

180. Wang, T.; Wang, S.; Cheng, Z.; Wei, J.; Yang, L.; Zhong, Z.; Hu, H.; Wang, Y.; Zhou, B.; Li, P. Emerging core–shell nanostructures for surface-enhanced Raman scattering (SERS) detection of pesticide residues. *Chem. Eng. J.* **2021**, *424*, 130323. [CrossRef]

181. Louppis, A.P.; Kontominas, M.G. Analytical insights for ensuring authenticity of Greek agriculture products: Unveiling chemical marker applications. *Food Chem.* **2024**, *445*, 138758. [CrossRef]

182. Ali, A.H. High-performance liquid chromatography (HPLC): A review. *Ann. Adv. Chem.* **2022**, *6*, 010–020.

183. Lu, S.Y.; Zhang, L.L.; Pan, J.R.; Yang, D.H.; Sui, Y.N.; Zhu, C. Cherry origin identification based on Raman spectroscopy combined with LSTM long short-term memory network. *Spectrosc. Spectr. Anal.* **2021**, *41*, 1177–1181.

184. Lu, S.Y. Study on Origin Traceability of Cherry Based on Raman Spectrum and Pattern Recognition. Master's Thesis, China University of Metrology, Hangzhou, China, 2021.

185. Traksele, L.; Snitka, V. Surface-enhanced Raman spectroscopy for the characterization of *Vaccinium myrtillus* L. bilberries of the Baltic–Nordic regions. *Eur. Food Res. Technol.* **2022**, *248*, 427–435. [CrossRef]

186. Arndt, M.; Rurik, M.; Drees, A.; Bigdowski, K.; Kohlbacher, O.; Fischer, M. Comparison of different sample preparation techniques for NIR screening and their influence on the geographical origin determination of almonds (*Prunus dulcis* MILL.). *Food Control.* **2020**, *115*, 107302. [CrossRef]

187. Wadood, S.A.; Boli, G.; Xiaowen, Z.; Hussain, I.; Yimin, W. Recent development in the application of analytical techniques for the traceability and authenticity of food of plant origin. *Microchem. J.* **2020**, *152*, 104295. [CrossRef]